NUMERICAL STUDY TO EVALUATE THE PERFORMANCE OF MICROCHANNEL HEAT SINK WITH DIFFERENT FLOW PATH CONFIGURATIONS

A PROJECT REPORT

Submitted by

RAGUL KRISHNA P (715517114040)

UVANPRASANTH S (715517114057)

DINESH BABU A K (715517114302)

RICHARD ALLEN PAUL F (715517114041)

In partial fulfilment of the award of the degree

Of

BACHELOR OF ENGINEERING

IN

MECHANICAL ENGINEERING

PSG INSTITUTE OF TECHNOLOGY AND APPLIED RESEARCH, COIMBATORE

ANNA UNIVERSITY: CHENNAI 600 025

MAY 2021

ANNA UNIVERSITY: CHENNAI 600 025

BONAFIDE CERTIFICATE

Certified that   this project   report "**NUMERICAL STUDY TO EVALUATE THE PERFORMANCE OF MICROCHANNEL HEAT SINK WITH DIFFERENT FLOW PATH CONFIGURATIONS**" is the bonafide work of **"RAGUL KRISHNA P, UVANPRASANTH S, DINESH BABU A K, RICHARD ALLEN PAUL F"** who carried out the project work under my guidance.

<table>
<tr><td>SIGNATURE</td><td>SIGNATURE</td></tr>
<tr><td>HEAD OF THE DEPARTMENT</td><td>SUPERVISOR</td></tr>
<tr><td>(Dr. N. Saravanakumar)</td><td>(Mr. Avinash Kumar. R)</td></tr>
<tr><td>Head of the Department,</td><td>Assistant Professor,</td></tr>
<tr><td>Department of Mechanical Engineering,</td><td>Department of Mechanical Engineering,</td></tr>
<tr><td>PSG Institute of Technology and</td><td>PSG Institute of Technology and</td></tr>
<tr><td>Applied Research, Neelambur, Coimbatore</td><td>Applied Research, Neelambur, Coimbatore</td></tr>
</table>

INTERNAL EXAMINER   **EXTERNAL EXAMINER**

ACKNOWLEDGEMENT

ABSTRACT

The flow path plays an important role in the performance of the microchannel heat sink. A good flow path design configuration may result in the higher thermohydraulic performance of the microchannel heat sink. The present study proposes microchannel heat sinks with different flow path configurations for various fin types and orientation. The various flow path configurations include straight microchannel, inclined fin microchannel and Rib type microchannel. A microchannel with hydraulic diameter 500 µm was used for the analysis with a heat flux of 10 W/cm^2. The CFD simulation is carried out for Laminar Region i.e. Reynolds number ranging from 200 to 1000. It was found that Inclined fin microchannel 90^0 possess better thermohydraulic performance than other type taken into consideration. The pressure drop is also higher for the inclined fin microchannel but the significance of pumping power is very less. Heat transfer coefficient of 90^0 inclined fin channel is 54% higher than Asymmetric rib channel of 8mm radius at Re=400 and 98% higher at Re=600.

CONTENTS   Page No.

LIST OF FIGURES

LIST OF TABLES

CHAPTER 1

INTRODUCTION

Recent development in semiconductor and other mini- and micro-scale electronic technologies and continued miniaturization have led to a very high increase in power density for high-performance chips. Although impressive progress has been made during the past decades, there remain serious technical challenges in thermal management and control of electronics devices or microprocessors. The two main challenges are: adequate removal of ever-increasing heat flux and highly non-uniform power dissipation.
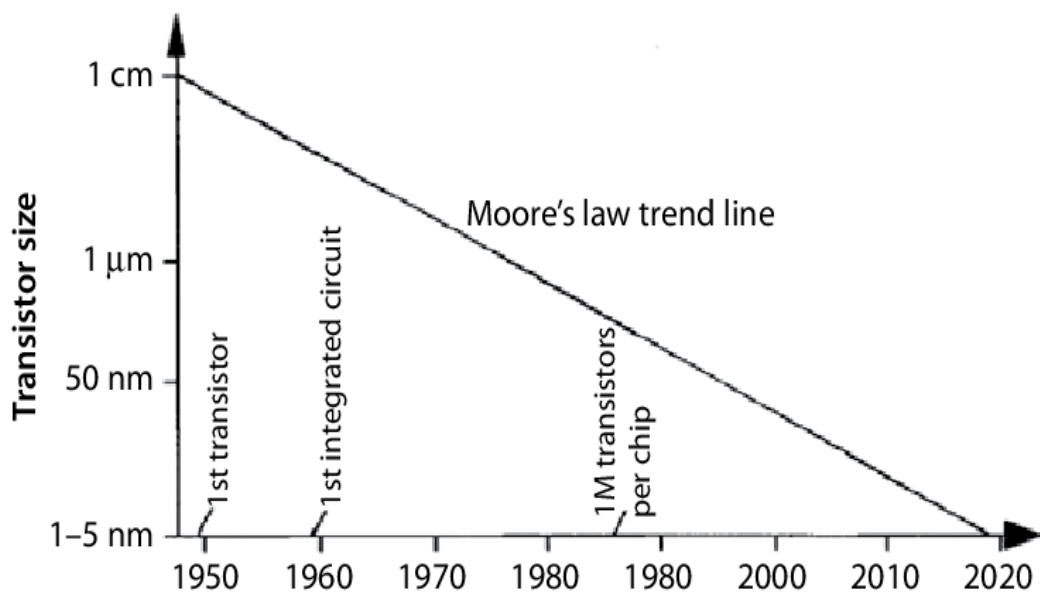
Fig 1.1 Development of Microelectronics

Thus, the heat generated within the devices has to be removed in order to avoid creation of hot spots that may shorten the life span of devices or even permanent damage of electronic components. Moore's Law, prediction made by American engineer Gordon Moore in 1965 states that the number of transistors on a microchip doubles every two years, as transistors in integrated circuits become more efficient, computers become smaller and faster. The below graph shows the Moore's law trend line shows the steep decrease in the transistor size along the years. There is an urgent need for high-performance heat sinks to ensure the integrity and long life of these petite systems. Use of forced convection cooling has been limited by the requirement of the excessively high flow velocity and associated noise and vibration problems. Microchannel heat sink seems to be the most reliable cooling technology due to its superior command over heat carrying capability.

1.1 Microchannel heat sink (MCHS)

A microchannel heat sink consists of very small channels and fins in a parallel arrangement. The heatsink is usually kept very close to the device that requires cooling; Heat from the active device to the heatsink through conduction. Heat transfer from the heat sink to the surroundings is achieved by passing a coolant, usually a liquid, through the channels.

1.2 Types of cooling systems
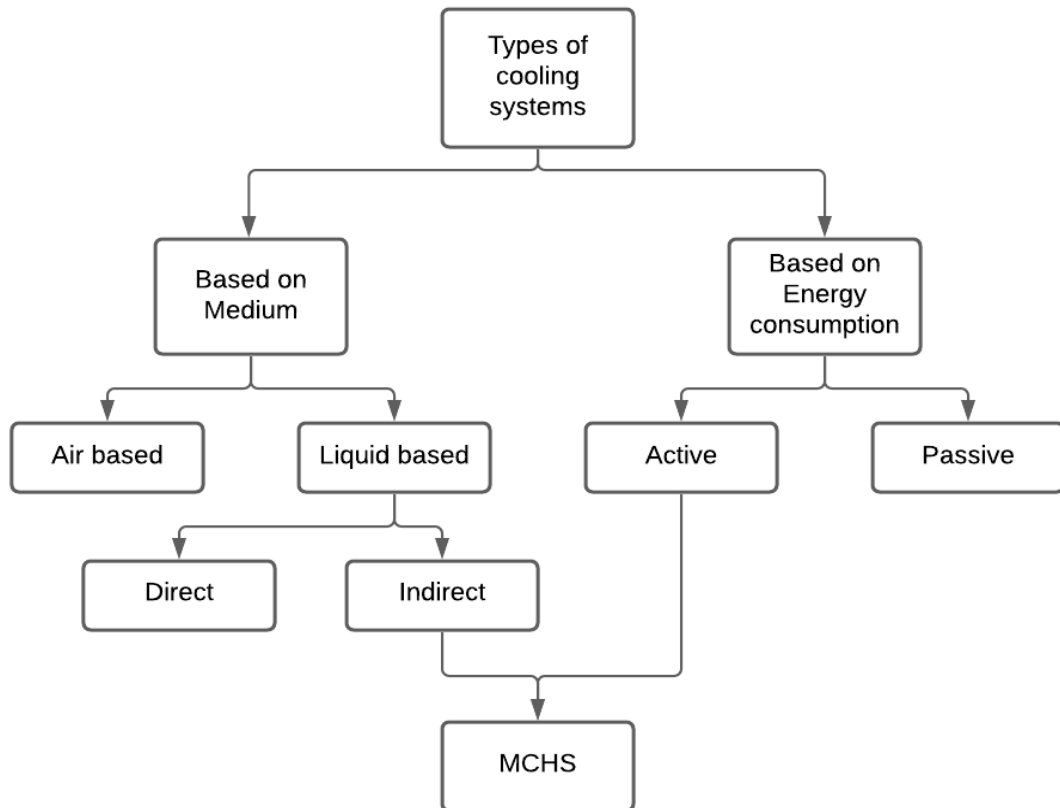
Fig 1.2 flowchart showing the classification of cooling systems

1.2.1 Air based cooling systems

Air is used as the medium of heat transfer. Natural convection, forced convection, thermoelectric coolers, forced air impingement comes under this category.

1.2.2 Liquid based cooling systems

Liquid is used as the medium of heat transfer. Commonly used liquids are water, refrigerants and nanofluids. Liquid based cooling systems are further divided into two categories namely

1. Direct based cooling systems
2. Indirect based cooling systems

Cooling classified based on energy consumption are:

1.2.3 Active cooling:

Active cooling is a heat-reducing mechanism that uses external energy like fans to reduce the heat of desired components.

1.2.4 Passive Cooling:

Passive cooling is a heat reducing mechanism that does not use any external source of energy to remove heat. It utilizes natural conduction, convection, and radiation to cool a component. Microchannel heat sinks come under the Active, Indirect method of cooling as the liquid does not physically come in contact with the part to be cooled.

1.3 Working of a Microchannel

In a Microchannel, the heated (bottom) wall comes in contact with the top surface of the microprocessor. The heat from the microprocessor is transferred to the heated wall and then absorbed by the water flowing through the channel. Thus, the outlet temperature of water is higher when compared to the inlet temperature as the effect of heat carried away by the fluid.
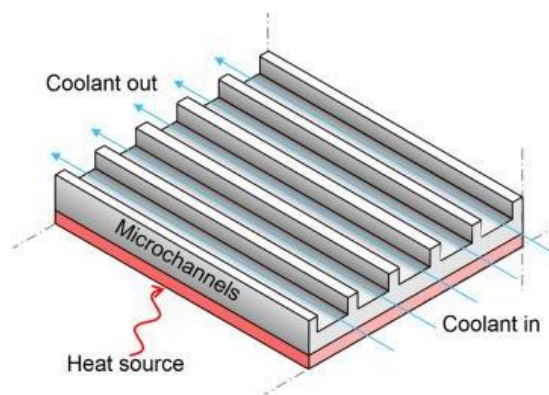
Fig 1.3 Microchannel Cross-section

Heat Balance $= m*C_p*(T_{out}-T_{in}) = h*A*(\Delta T)$

1.4 Objective

The aim of the project is to design a suitable Microchannel flow path to enhance the thermo-hydraulic performance.

1.5 Project Description

This project aims to develop a microchannel configuration with maximum heat transfer and minimum pressure drop with water as coolant.

1.6 Inference from Past work

1. The size of the micro channel heat sink was decided based on the size of the microprocessor. Processor used: **"INTEL CORE i9 10940X".**

2. In order to obtain a proper flow distribution, different inlet and outlet manifolds were varied with the geometry dimensions and positions.

3. The header configuration doesn't have much effect on the flow distribution among the channels. **Side inlet has the low pressure drop** among the different configurations used.

4. Header diameter has a larger effect on the flow distribution. **Inner diameter of 5.1 mm** was selected because of better flow distribution and **minimum pressure drop.**

5. Header length does not have any significant effect on the flow distribution

6. As the number of channels increases pressure drop and maximum temperature decreases. **N=74** was selected because of **higher heat transfer coefficient.**
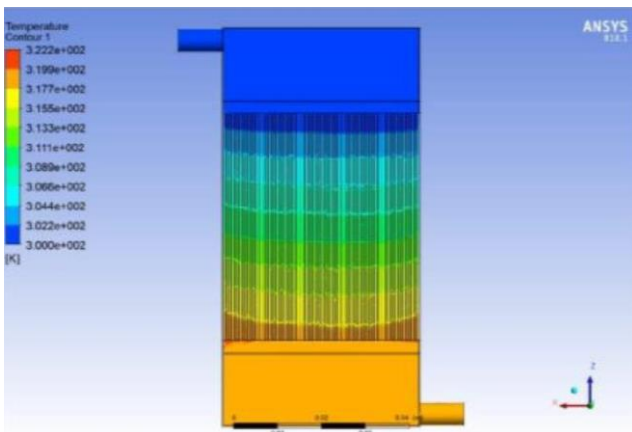
Fig 1.4 Temperature Contour of Microchannel   *Fig1.5 Velocity Contour of the Microchannel*
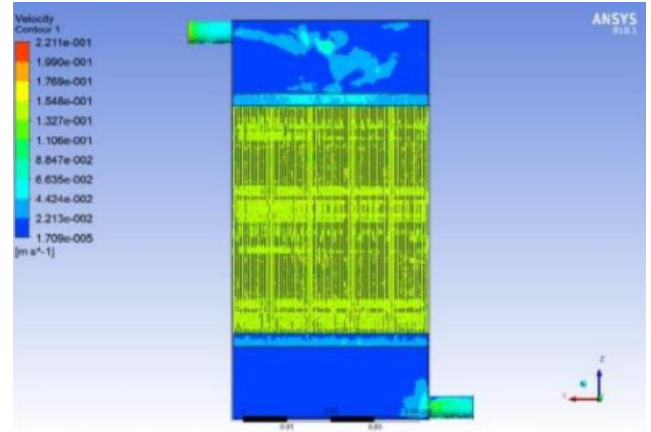
CHAPTER 2

LITERATURE REVIEW

This chapter provides the details of studies conducted on micro channel heat sink. It is essential to look for efficient cooling solutions to meet the cooling demands of the latest high-power devices which have high heat flux that has to be effectively dissipated. Following literature describes the heat transfer characteristics of micro channel heat sink.

Yogesh K. Prajapati et al., (2019) [1] conducted CFD simulations studying the Influence of fin height on heat transfer and fluid flow characteristics of a rectangular microchannel heat sink. The simulations have been studied with rectangular parallel microchannel heat sink by varying fin height. 7 different fin heights varying from 0.44 to 1mm have been used. Numerical 3D simulations were carried out by varying the heat flux from 100 to 500KW/m^3 and Reynolds no from 100 to 400. Single phase liquid water is used as coolant to remove heat from the sink. It has been found that the Optimum fin height of 0.8 mm has higher heat transfer rate. Since it is an open type, flow distribution is uniform throughout the microchannel.

Dawei Zhuang et al., (2020) [2] performed the optimization of Microchannel Heat Sink with Rhombus Fractal-like Units for Electronic Chip Cooling. A novel structure of microchannel heat sink with rhombus fractal-like units is proposed to improve the overall performance, and a geometry optimization approach is developed for the design of the new microchannel heat sink. For validating the reliability of the proposed design approach, the results predicted by the calculation method of pumping power are compared to the experimental data under two types of RMCHS samples and various working conditions The inlet water velocities u_0 range from 0.25 m/s to 2 m/s with a step size of 0.25 m/s; the maximum wall temperatures range from 343K to 358K with a step size of 3K. The inlet water temperature is set as 298K, and the heat flux is specified as 20 W/cm^2.It was found that the rhombus fractal-like units may increase the COP by 7.9%- 68.7%, and may effectively improve the cooling efficiency of Microchannel heat sinks. Pumping power is less for this case than the conventional Microchannels.

K. Derakhshanpour et al., (2020) [3] studied new designs for ribbed micro channels (semi-circular and semi-elliptic) and filleted ribs. Four different configurations were taken and the effects of rib shape and rib fillet on thermal performance and pressure

drop in micro channels can be investigated in these configurations with water as the coolant used. Effect of filleted ribs is found to be more effective in improving total performance in comparison with the shape of ribs. Filleted ribs can lower the bottom surface temperature by reducing the stagnation zone effect and redirecting fluid flow toward channel walls. In Microchannel with semi-elliptic ribs and filleted corner configurations, Nusselt number increases from 18–21%, Filleted ribs can lower the bottom surface temperature by reducing the stagnation zone effect and redirecting fluid flow.

Fei Li et al., (2020) [4] studied heat transfer and flow characteristics of microchannels with solid and porous ribs by investigating comprehensively using numerical approaches. It is reported that the thermal performance of microchannels with solid and porous ribs are significantly better than those without any ribs. the average temperatures of the bottom surface at Re = 100 along the flow direction (x direction) for all cases are calculated. As a whole, the cases with porous ribs have a higher Nusselt number than the cases with solid ones; the extra convective heat transfer occurs in porous regions, which improves the heat dissipation.

Shi Zeng et al., (2020) [5] conducted an experimental and numerical study on Topology optimization of liquid-cooled microchannel heat sinks. The process of designing liquid-cooled microchannel heat sink fin geometries based on a numerical method, topology optimization is done and the parameter study for different velocities and junction temperature constraints is performed. The performance comparison shows that the topology optimized heat sinks could save up to 50.9% pumping power under the same thermal performance requirement. The heat sink is subjected to a constant heat flux from the bottom surface and a constant water flow rate. In terms of performance evaluation criteria, lower bottom surface average temperature and lower pressure drop to drive the water are considered favorable. The generated heat sink structures are non-conventional and show better performance in comparison with size optimized SC heat sinks. The 3D numerical simulation method presented in this paper is proved to be accurate in predicting performance of microchannel to heat sinks. The pressure and temperature prediction errors compared to experimental data are less than 6% and 1 Deg C, respectively.

Qi Feng Zhu et al. (2020) [6] studied Fluid flow and heat transfer characteristics of microchannel heat sinks with different groove shapes. The effect of channel geometry on overall performance was studied to understand the fluid flow and

heat transfer characteristics of microchannel heat sinks having groove sidewalls. A three-dimensional computational fluid dynamics model was developed, validated, and used to optimize the geometric structure. Comparisons were made between different groove shapes in order to determine the optimum structure. The results indicated that the overall performance can be greatly improved by arranging grooves on channel sidewalls. The thermal enhancement efficiency of all the grooved-channels increases with increasing the Reynolds number except that of the rectangular grooved-channel. The triangular grooved-channel can achieve the highest thermal enhancement efficiency, but the water droplet grooved-channel possesses the greatest potential for further improving thermal enhancement efficiency.

Nicholas Gilmore et al., (2020) [7] studied the open manifold microchannel heat sink for high heat flux electronic cooling with a reduced pressure drop. This study considers a conventional manifold microchannel heat sink, it consists of two layers: an upper layer of manifold channels and a lower layer of microchannels. Inlet and outlet manifold channels are interdigitated with each other, running inwards from opposite sides of the heat sink. Compared to the baseline geometry, the open geometry substantially reduced the pressure drop, with only a slight increase in thermal resistance. The open geometry also retained the benefits of a conventional manifold microchannel heat sink: low thermal resistance, thin profile, liquid waste heat recovery and a simple planar geometry well suited to microfabrication.

Liang et al., (2019) [8] studied the effect of flow rate, heat flux, fluid inlet temperature on the performance of micro channel heat sink. He developed a standard k-ε turbulence computational fluid dynamics model and simulated it for heat transfer characteristics of micro channel. He compared the results obtained from the computational and experimental studies. He found a good agreement between those two studies. From the results obtained he concluded that as the flow rate increases the temperature difference decreases and the pressure drop increases; as the heat flux increases the temperature difference increases. The inlet fluid temperature does not have a greater effect on the heat transfer.

Sanjeev Kumar et al., (2019) [9] studied the effects of flow inlet angle on flow maldistribution and thermal performance of water cooled mini-channel heat sink. They considered a micro channel heat sink with 28 number of parallel mini channels having a hydraulic diameter of 1.5mm. Water was used as the working fluid and aluminum was chosen as heat sink material. With the help of ANSYS-Fluent, they numerically analyzed

the micro channel heat sink for different flow inlet angles such as ($\theta=90°$, $\theta=105°$, and $\theta=120°$). From this study they suggested that the performance of a mini channel heat sink can be improved if coolant enters the distributor header with flow inlet angle $\theta=105°$ and exit from the middle of the collector header.

Vikas Yadav et al., (2016) [10] performed a numerical investigation of heat transfer in extended surface microchannels. The heat transfer enhancement in microchannel using extended surface has been carried out. Rectangular microchannel and cylindrical micro fins are used in current study. Three different configurations of extended surface microchannel; Case I (upstream finned microchannel), Case II (down-stream finned microchannel) and Case III (complete finned microchannel) are compared with plain rectangular microchannel. It is found that heat transfer performance of Case I is better than Case II. Case I even performs better than Case III at low Reynolds number. Average surface temperature is also significantly reduced in case of extended surface microchannels. Overall performance is higher for Upstream finned MC at lower Reynolds number and when Reynolds number is high, performance is greater for Completely Finned MC. Nusselt number increases by 160% when fin is modified.

Ergin bayrak et al., (2018) [11] studied the effects of geometric structure of microchannel heat sink on flow characteristics and heat transfer performance Comparative analysis was performed to determine which design is the best in terms of the heat transfer, the pressure drop, the overall performance and the temperature distribution on the baseline wall. It was observed that local modifications in channels can ensure suitable fluid mixing between core flow and near wall regions; therefore, this situation enhances heat transfer performance considerably compared to Microchannel heat sink with no cavity and rib. Microchannel with symmetric cavity and rib is best in terms of heat transfer and overall performance. Jetting and throttling effect is dominant. Base temperature distribution is uniform for microchannel with asymmetric cavities which are 40% higher than others.

Hua Ma et al., (2021) [12] performed numerical investigation to study the heat transfer characteristics of laminar flow in three-dimensional rectangular microchannels with aspect ratios of 0.1–1 and Reynolds numbers of 5–400. The effects of aspect ratio and Reynolds number on the local and mean Nusselt numbers are presented in detail. The results show that the Reynolds number has a great impact on the local Nusselt number in the thermally developing region, especially at lower Reynolds number, while the Reynolds number is independent of the developed Nusselt number. The local Nusselt

number is found to increase with decreasing aspect ratio at the same Reynolds number. Thermal performance of rectangular microchannels can be predicted quickly and easily through the use of the developed correlations for the thermal entrance length and the Nusselt number for different Reynolds numbers, aspect ratios, and channel lengths.

V. Murali Krishna et al., (2021) [13] carried out a numerical study to examine the heat transfer and pressure drop characteristics for laminar flow of hybrid nanofluid as a coolant in a circular micro-channel heat sink under forced convection conditions The performance of heat sink is evaluated using Multi-Walled Carbon Nanotubes (MWCNT)-CuO/water based hybrid nanofluid for different mass flow rates, with the volume fractions ranging from 1% to 3%. The law of mixtures and correlations existing in the literature are used to find the properties of hybrid nanofluids. The influence of Reynolds number on pumping power and the heat transport rate is studied for different mixture ratios of MWCNT-CuO/water-based hybrid nanofluids and similar studies were carried out for MWCNT-water and CuO-water mono fluids. The results show a step up in heat transfer with hybrid nanofluids over mono nanofluids and the enhancement of heat transfer is observed with rise in volume fraction.

Guilian Wang et al., (2020) [14] conducted a Numerical study to examine the heat transfer characteristics of a microchannel heat sink (MCHS) with truncated ribs (TRs) on the sidewall for Reynolds number ranging from 100 to 1000. Three parameters of the TR configuration -gap height, rib arrangement and rib width - are selected to analyze the effects of rib geometry on the hydrothermal performance. It is found that, either in the staggered cases or parallel cases, the TRs can improve the heat transfer near the truncation gap and largely decrease the overall pressure drop. Therefore, the existence of TR can improve the overall thermal performance by reducing the pressure drop penalty without heat transfer loss.

Yaw-Jen Chang et al., (2017) [15] carried out a study on five different channel shapes using a novel scheme for meshing and a structure of a multi-nozzle microchannel heat sink. a copper plate measuring 9.8 mm × 9.8 mm × 0.5 mm was used as a fixed substrate for designs with single-layer-and-parallel or multi-nozzle microchannel heat sinks. Water was applied as the coolant. Channel lengths from 0.2 to 5.6 mm and five different channel shapes, including a circle, square, trapezium, two concave surfaces, and two convex surfaces, were numerically investigated in detail at a constant hydraulic diameter of 200 μm with a Reynolds number in the range of 700–2200. For all cases in this study, it was found that the best thermal performance was achieved with a circular

channel shape which could dissipate a heat flux up to 1500 W/cm^2, and the maximum temperature was kept at less than 75 °C at a Reynolds number of 2200.

Ihsan Ali Ghani et al., (2017) [16] reported the influence of channel zone related geometrical parameters such as corrugated channel and flow disruption (FD) on the hydrothermal performance (HP) of microchannel heat sink (MCHS). For efficient cooling, various channel shapes such as sinusoidal wavy, zigzag and convergent-divergent are introduced. The wavy MCHS with sinusoidal shape achieved a high rate of HT with acceptable levels of PD compared with other shapes of zigzag and convergent-divergent MCHS. These features are manifested in increasing the HT area, induction of better fluid mixing and formation CA. The most important characteristic within flow disturbance techniques is found in interrupted-wall channels which manifest low PD. It is established to be the most desirable feature in MCHS applications due to its role in reducing the pump power and liquid leakage risk.

Liaofei Yin et al., (2019) [17] studied heat transfer and pressure drop characteristics of water flow boiling in open microchannels. Experiments were conducted to investigate the heat transfer and pressure drop characteristics during flow boiling of deionized water (DI water) in open microchannels and to analyze the effects of operating conditions and channel dimensions. The experiments were carried out with the inlet subcooling ΔT sub = 20, 35, 50 °C at different mass fluxes ranging from 174 to 374 kg/m^2 s for varied applied heat flux 214.9–1355.1 W/cm2. Two open microchannel samples with different geometry dimensions were tested. Results showed that the onset of stratified flow (OSF) denoted an alternation of dominant heat transfer mechanism at which the heat transfer coefficient (HTC) was largest during the flow boiling.

Liangbin Su et al., (2020) [18] studied the heat transfer characteristics of thermally developing flow in rectangular microchannels with constant wall temperature. The effects of Reynolds number and aspect ratio on heat transfer properties have been calculated numerically. The local Nusselt number is found to be quite sensitive to the Reynolds number, especially for small Reynolds numbers. The slope of the Nusselt number curve is steeper with a lower Reynolds number when close to the inlet. It is found that the local Nusselt number is independent of the cross-sectional geometry at the channel inlet and the discrepancy of the local Nusselt number for different aspect ratios is gradually magnified along the streamwise direction. In consideration of the effects of Reynolds number and aspect ratio, new correlations are developed for actual Nusselt number and thermal entrance length of rectangular channels.

CHAPTER 3
DESIGN OF MICROCHANNEL HEAT SINK

The size of the Microchannel heat sink was decided based on the size of the microprocessor.

3.1 Microprocessor Specifications

Microprocessor name = INTEL CORE i9 10940X

Length = 52.5 mm

Width = 45 mm

Thermal design power (TDP) = 165 W

Safe operating temperature = 85 °C

Heat flux (Q) = TDP/Area = 10 W/cm^2

3.2 Modelling

Microchannel is a heat sink with a hydraulic diameter lesser than 1mm through which the fluid enters and removes the heat. A Straight Microchannel with a rectangular cross section (0.5 mm X 0.5 mm), hydraulic diameter 0.5 mm and a length of 52.5 mm was designed with no restrictions in the flow path. The wall thickness of the microchannel is 0.15 mm. The initial length of the microchannel (2.5mm) is intentionally left empty to avoid reverse flow. The flow path of the Microchannel has been modified into two different types,
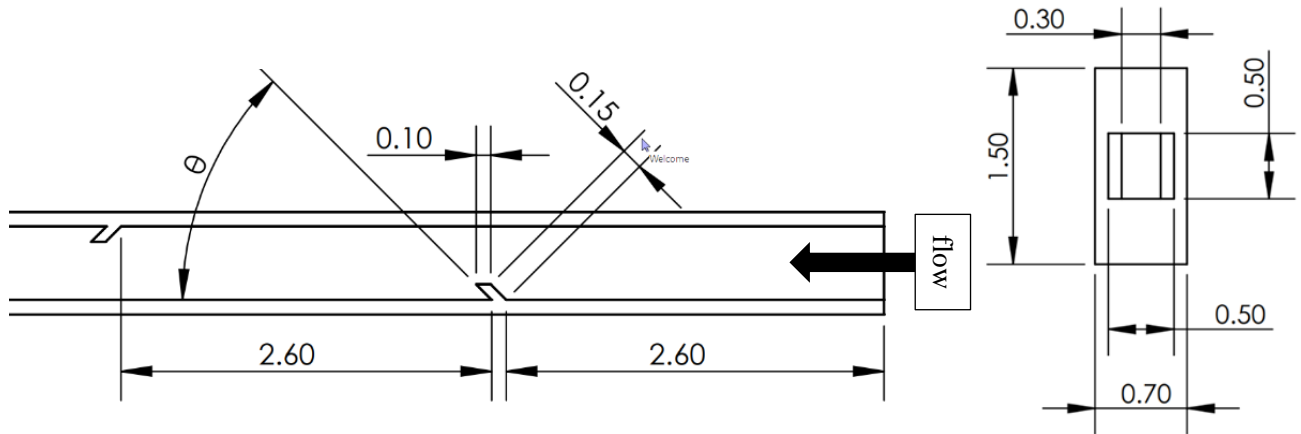
1. Inclined fin Microchannel
2. Ribbed Microchannel

       a) Symmetric Ribbed Microchannel

       b) Asymmetric Ribbed Microchannel

3.2.1 Inclined fin Microchannel

Inclined fin Microchannel was designed by introducing extended fins of trapezoidal section alternatively with dimensions 0.1 x 0.15mm along the side walls of the Microchannel flow path.

The inclination of the fins was varied from $\theta = 45°, 60°, 90°, 120°, 150°$, where θ is the inclination angle between the Side wall of the Microchannel and the extended fin. Inclined fin Microchannel Nomenclature is shown in below image.


Fig 3.1 Figure Showing Inclined Channel Nomenclature

In an inclined fin microchannel, the total number of fins is 19. One side of the microchannel consists 9 fins and the other side consists 10 fins, to make the design configuration uniform and to make it adjacent to each other. This inclined adjacent fin design eliminates the reverse flow which leads to an enhanced fluid flow. Pumping power is also increased due to this inclined pattern microchannel.

3.2.2 Ribbed Microchannel
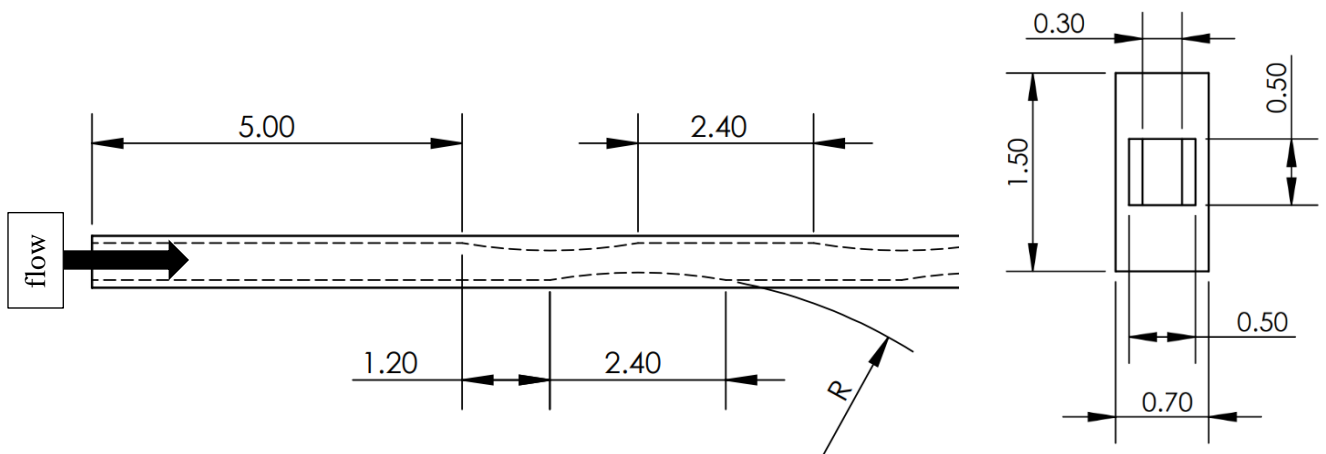
a. Symmetric Ribbed Microchannel

Symmetric Ribbed Microchannel was designed by introducing extended ribs of semi-circular section along the side wall of the Microchannel flow path. The ribs were placed parallel to each other and looks symmetrical along the axis of the Microchannel flow path. The rib fillet radius was varied for 6mm, 7mm and 8mm. Symmetric Ribbed Microchannel is shown in the below image. The total number of ribs in the channel are 20, either side consists of 10 ribs.
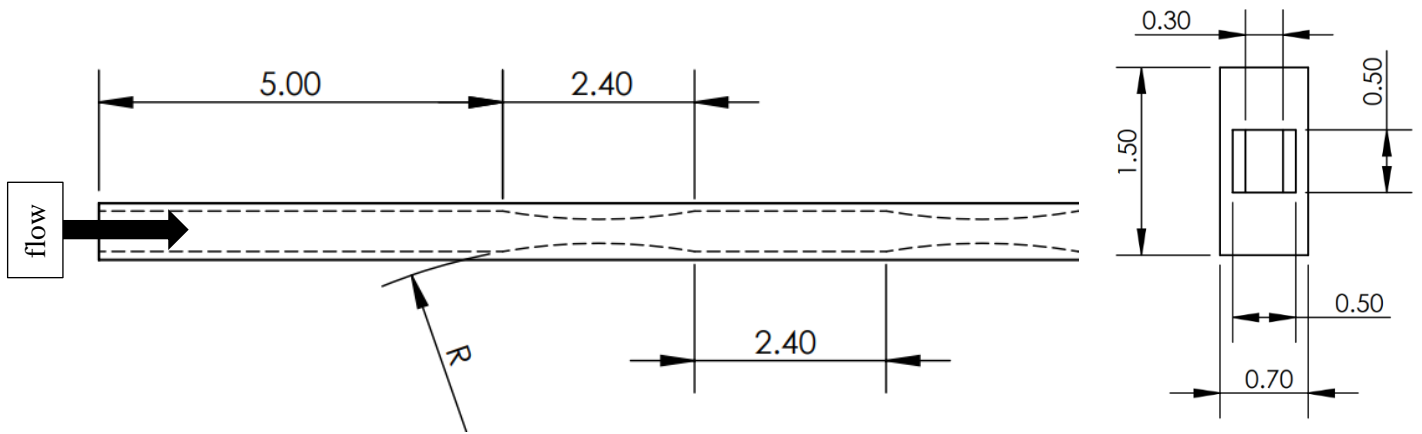
Fig 3.2 Symmetric Ribbed Microchannel

b. Asymmetric Ribbed Microchannel

Asymmetric Ribbed Microchannel was designed by introducing extended ribs of semi-circular section along the side walls of the Microchannel flow path. The ribs were placed alternative to each other and asymmetrical to the axis of the Microchannel flow path. The rib fillet radius was varied from 6mm, 7mm and 8mm. Asymmetric Ribbed Microchannel with different rib fillet radius is shown in the below image.

Fig 3.3 Asymmetric Ribbed Microchannel

The total number of ribs in the channel are 19, either side consists 9 ribs and 10 ribs. The flow cross-sectional area tends to increase and decrease simultaneously throughout the length of the channel.

<div align="center">**CHAPTER 4**</div>

<div align="center">**METHODOLOGY**</div>

Analysis in ANSYS Fluent: Conjugative Heat Transfer Analysis

4.1 Geometry

The required geometry has been imported to Ansys workbench (Fluent). The internal volume for fluid path has been created using space claim to create volume

4.2 Mesh

The default mesh available in ANSYS workbench is used to create the initial mesh the contact region of internal volume and the Microchannel is furnished with the fine mesh to obtain better results and equally divided into 45 number of divisions. The element size used 80μm. The element size used for the external volume is 80 μm. Named selection for inlet, outlet, top wall, bottom wall, and side walls where created
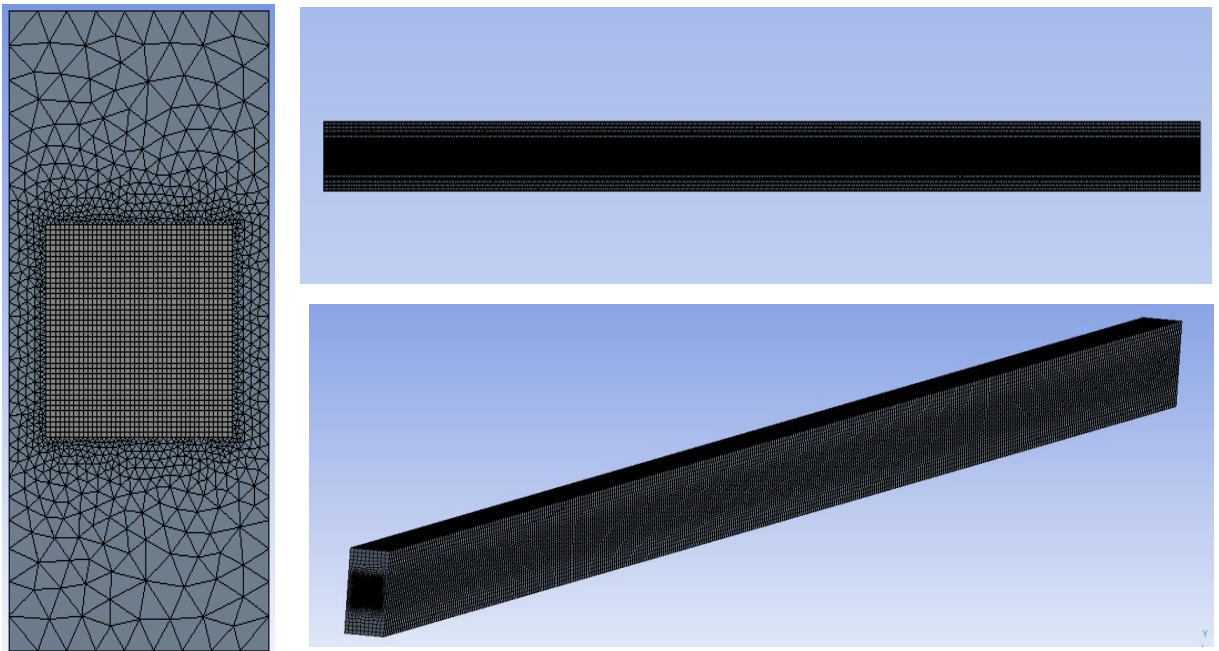
<div align="center">**Fig 4.1 Mesh Image for a Microchannel**</div>

4.3 Setup

Analysis performed: Conjugative heat transfer analysis

Continuity equation

$$\frac{\partial u}{\partial x} + \frac{\partial u}{\partial y} + \frac{\partial u}{\partial z} = 0$$

Momentum equation

Z- Momentum equation

$$\rho\left(u\frac{\partial w}{\partial x} + v\frac{\partial w}{\partial y} + w\frac{\partial w}{\partial z}\right) = -\frac{\partial p}{\partial z} + \mu w\left(\frac{\partial^2 w}{\partial x^2} + v\frac{\partial^2 w}{\partial y^2} + w\frac{\partial^2 w}{\partial z^2}\right)$$

X- Momentum equation

$$\rho\left(u\frac{\partial u}{\partial x} + v\frac{\partial u}{\partial y} + w\frac{\partial u}{\partial z}\right) = -\frac{\partial p}{\partial x} + \mu w\left(\frac{\partial^2 u}{\partial x^2} + v\frac{\partial^2 u}{\partial y^2} + w\frac{\partial^2 u}{\partial z^2}\right)$$

Y- Momentum equation

$$\rho\left(u\frac{\partial u}{\partial x} + v\frac{\partial u}{\partial y} + w\frac{\partial u}{\partial z}\right) = -\frac{\partial p}{\partial x} + \mu w\left(\frac{\partial^2 v}{\partial x^2} + v\frac{\partial^2 v}{\partial y^2} + w\frac{\partial^2 v}{\partial z^2}\right)$$

Energy equation

$$\rho Cp\frac{DT}{Dt} = k\,\nabla^2 T$$

4.4 Nomenclature

m $\quad$ = mass flow rate of the fluid (Kg/s)

T_{in} $\quad$ = inlet temperature of fluid (K)

C_p $\quad$ = Specific heat of the fluid (KJ/Kg. K)

A $\quad$ = Heat transfer area of Microchannel (m^2)

T_{out} $\quad$ = outlet temperature of fluid (K)

T_w $\quad$ = wall temperature (K)

T_f $\quad$ = average fluid temperature (K)

Q $\quad$ = Volumetric flow rate (m^3/s)

ΔP $\quad$ =Pressure drop across channel (Pa)

Tmax = Chip Maximum Temperature (K)

Tmin = Ambient Temperature (K)

q $\quad$ = Heat flux (W/m$^{2)}$

D_h $\quad$ = Hydraulic diameter (m)

ρ $\quad$ = Density of the fluid (kg/m^3)

U_m $\quad$ = Mean Velocity of the Fluid (m/s)

L_t = Length of the Microchannel (m)

U_{in} = Inlet velocity of the fluid (m/s)

P_{out} = Outlet Pressure (Pa)

W_t = Width of the microchannel (mm)

Pp   = Pumping Power (Watts)

f   = friction factor

4.5 Validation

The present study is validated with Effect of rib shape and fillet radius on thermal-hydrodynamic performance of microchannel heat sinks done by Derakhshanpour et al. This validation studies the base temperature of the channel along the length.

Boundary Conditions:

Table 4.1 showing Validation Boundary Conditions for different zones

Zone	Boundary Conditions	Expression
Inlet	Velocity-inlet	$Z = 0$; $u_{in} = 1$ m/s, $T_{in} = 293K$
Outlet	Pressure- outlet	$Z = L_t$: $P_{out} = 0$ (gauge pressure)
Bottom Wall	Constant Heat Flux	$Y = 0$: $-K_s\dfrac{\partial Ts}{\partial z} = q = 10^6$ W/m^2
Left and Right Walls	Symmetry	$X = 0$ & $X = W_t/2$: $\dfrac{\partial Ts}{\partial z} = 0$
Other Walls	Adiabatic	$\dfrac{\partial Ts}{\partial z} = 0$, $\dfrac{\partial Tf}{\partial z} = 0$

Fig 4.2 showing Validation graph between present and Derakhshanpour's study
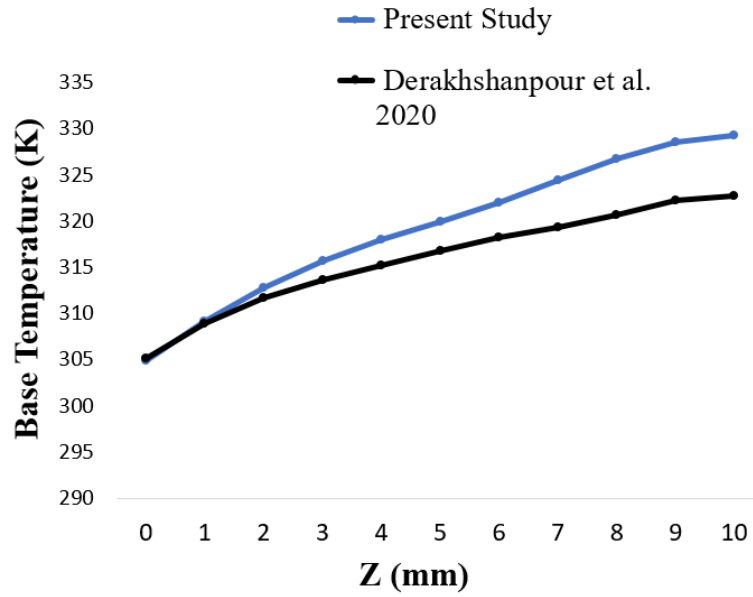
As shown in the graph, the base temperature for the present study is aligned with Literature's study. Maximum variation was found at the exit of Microchannel which is 2.02%.

4.6 GRID INDEPENDENCE STUDY

Before running any CFD simulation it is necessary to perform a grid independence study to make sure that the results of the analysis are not dependent on chosen grid. Grids with 148388 nodes, 230000 nodes, 450917 nodes and 702365 nodes are considered to test the grid independence of the solution. Chip maximum temperature is compared for different nodes. It was observed that the 702365 nodes and 450917 nodes have almost similar chip maximum temperature. 450917 nodes were considered for all the simulation due to less computing time and less allocated memory by the solver.

Table 4.2 showing Variation of chip maximum temperature with different nodes

Nodes	Chip Maximum Temperature (^{o}C)
148388	336.506
230000	337.88
450917	338.063
635702	338.069

4.7 Assumptions Taken

To simplify the analysis following are the some of the assumptions considered
- Steady state 3D flow
- Radiation heat transfer can be neglected
- Incompressible flow
- Laminar flow
- Single phase

The physical properties of water at 30° C is shown in Table below

Table 4.3 Showing Fluid Properties

Density (kg/m^3)	Thermal conductivity (W/m K)	Viscosity (m^2/s)
997	0.6071	8.502E-5

4.7 Boundary Conditions

Table 4.4 showing CFD Boundary Conditions

Zone	Boundary Conditions	Expression
Inlet	Velocity-inlet	$Z = 0$; $u_{in} = [0.341, 0.642, 1.023, 1.364, 1.705]$ m/s, $T_{in} = 293K$
Outlet	Pressure- outlet	$Z = L_t$: $P_{out = 0}$ (gauge pressure)
Bottom Wall	Constant Heat Flux	$Y = 0$: $-K_s\frac{\partial Ts}{\partial z} = q = 10^6$ W/m^2
Left and Right Walls	Symmetry	$X = 0$ & $X = W_t/2$: $\frac{\partial Ts}{\partial z} = 0$
Other Walls	Adiabatic	$\frac{\partial Ts}{\partial z} = 0$, $\frac{\partial Tf}{\partial z} = 0$

4.8 Numerical Schemes

The pressure-based solver of ANSYS FLUENT 18.1 is used for the analysis. The specific schemes used for the different terms in the equations are listed below

1. Solution scheme: SIMPLEC Algorithm
2. The residuals for continuity, momentum, and energy are set to be 10^{-6}, 10^{-6}, 10^{-9} respectively

4.9 Model Calculation for Inclined Channel 45º

1. Heat transfer coefficient (W/m² K)

Heat transfer coefficient, (h) $\quad = \dfrac{m*cp*(Tout-Tin)}{A*(Tw-Tf)}$

Heat transfer Area, A = Length of microchannel * Width of the Microchannel

$$= \dfrac{8.50E-05 * 4.18E+03 * (310.337-300)}{2.63E-05 * (311.26 - 303.05)}$$

h = 17045.88 W/m² K

2. Pumping power (W)

Pumping power, (Pp) $\quad = \dfrac{m * \Delta P}{0.7* \rho}$

$$= \dfrac{8.50E-05 * 2100.46}{0.7* 200}$$

Pp = 0.0003 W

3. Friction Factor

Friction Factor, (f) $\quad = \dfrac{\Delta P*Dh}{2* \rho * Lt * Um}$

$$= \dfrac{2100 * 0.0005}{2* 200 * 5.25E-04 * 0.67}$$

f = 0.0150

4. Coefficient of Performance

Coefficient of Performance, (COP) $\quad = \dfrac{Heat\ Transfer\ coefficient}{Pressure\ Drop}$

$$= \dfrac{17045.88}{2100.46}$$

COP = 8.1153

CHAPTER 5

RESULTS AND DISCUSSION

The suitable flow path of the microchannel was selected based on three parameters namely pressure drop, heat transfer coefficient and friction factor. Pressure drop and friction factor should be minimum. Heat transfer coefficient should be maximum.

5.1 Straight Microchannel

The geometry is simple in the case of straight microchannel which does not have any flow restriction in the design. So, the performance of the channel is minimum. Heat transfer rate and pressure drop is minimum as compared to inclined fin type and ribbed fin type microchannel. As the Reynolds number increases from 200 to 1000, the heat transfer coefficient and pressure drop keeps increasing. Because of this trend, Coefficient of performance decreases.

Figure 5.1 to 5.10 shows the temperature and velocity contours for the straight microchannel for the Reynolds number ranging from 200 to 1000.

Table 5.1 to 5.6 shows the Variation of heat transfer coefficient, pressure drop, outlet temperature and Coefficient of performance with respect to Reynolds number for straight and Inclined fin Microchannels.

Table 5.1 Results for Straight Microchannel

S. No	Reynolds No	Outlet temperature	Heat transfer coefficient	Pressure drop	COP
	-	K	W/m^{2}K	Pa	
1	200	310.34	13190.07	1833.67	7.19
2	400	305.17	16350.49	3837.34	4.26
3	600	303.45	19140.85	6005.04	3.19
4	800	302.59	21569.69	8327.09	2.59
5	1000	302.07	23625.55	10802.60	2.19
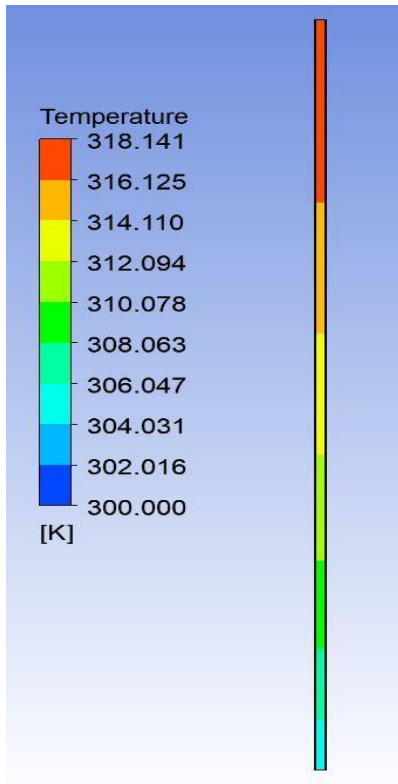
Fig 5.1 Temperature contour SC Re=200
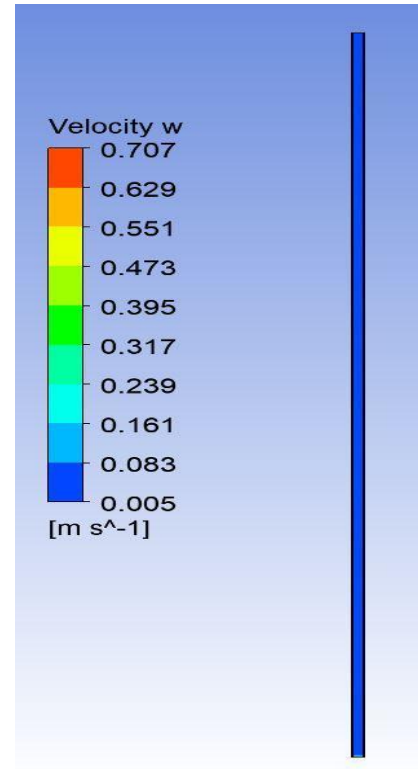
*Fig 5.2 Velocity contour SC Re=200*
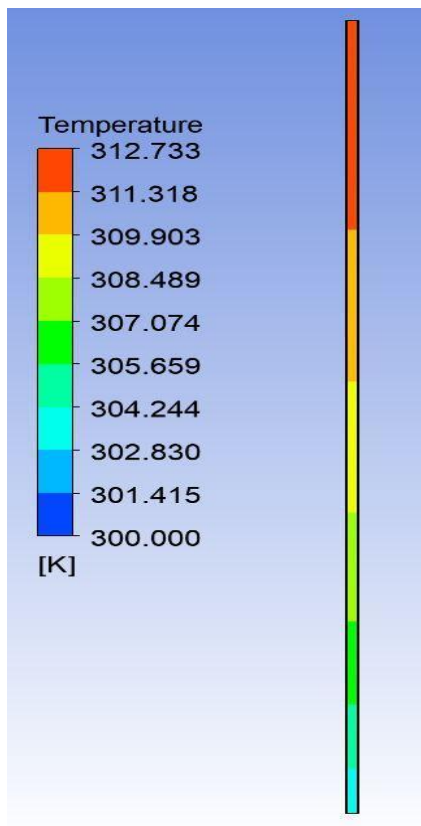
Fig 5.3 Temperature contour SC Re=400
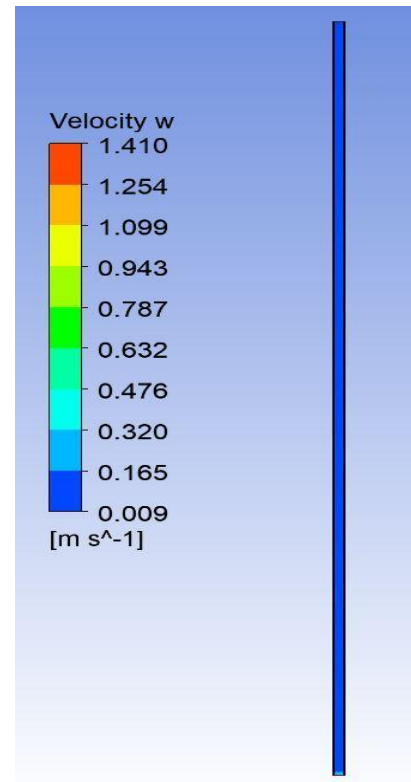
Fig 5.4 Velocity contour SC Re=400

21
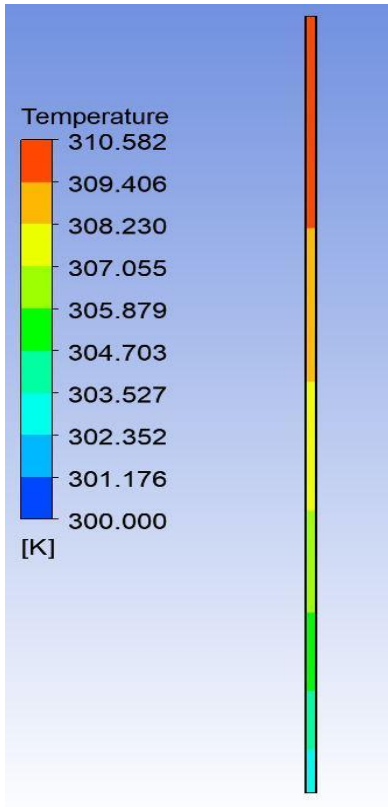
**Fig 5.5 Temperature contour SC Re=600**
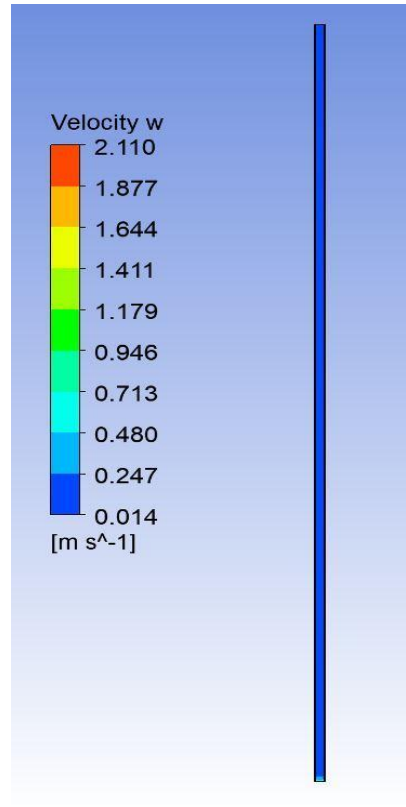
**Fig 5.6 Velocity contour SC Re=600**
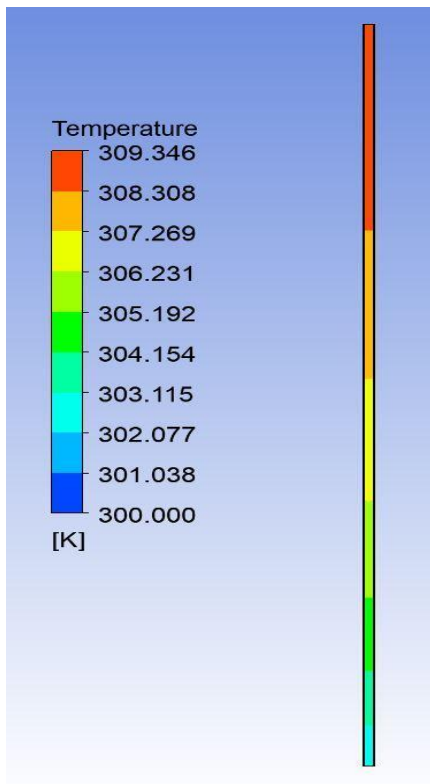
Fig 5.7 Temperature contour SC Re=800
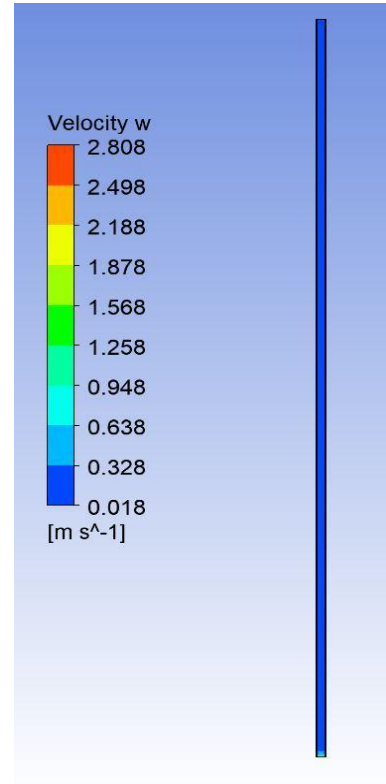
Fig 5.8 Velocity contour SC Re=800
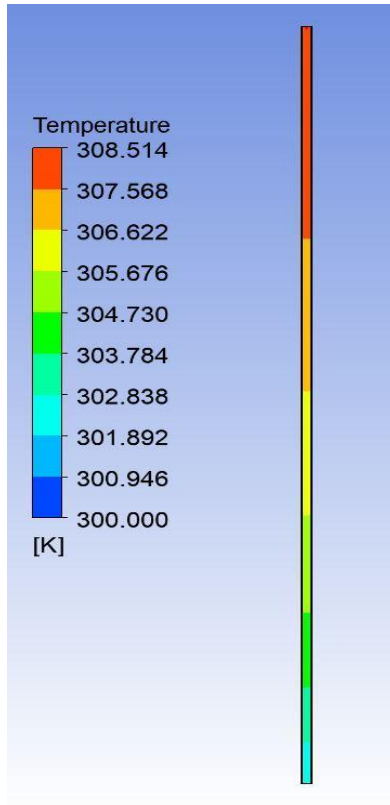
Fig 5.9 Temperature contour SC Re=1000   *Fig 5.10 Velocity contour SC Re=1000*
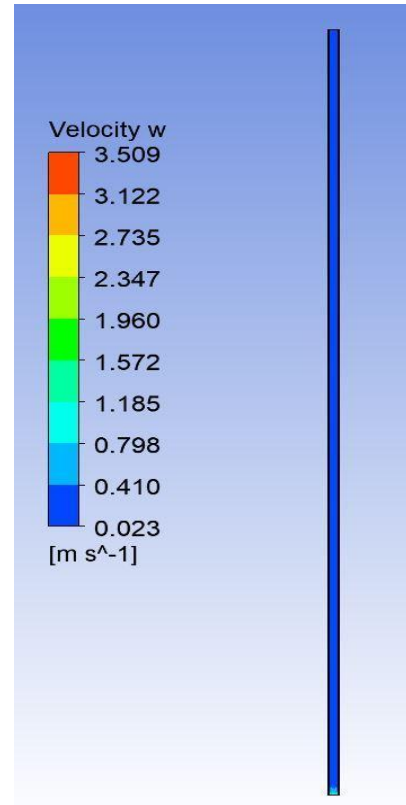
5.2 Inclined fin Microchannel

In this type of microchannel, trapezoidal section fin is introduced in the flow path of the microchannel which is oriented to the wall. The orientation angle varies from 45 degree to 150 degree as shown in the figure 3.1. The heat transfer coefficient of this Microchannel is better than the Straight microchannel but the Coefficient of performance is lesser than the straight microchannel because of the increase in pressure drop for higher Reynolds number. Figure 5.11 to 5.60 shows the temperature and velocity contours for the Inclined fin microchannel for the Reynolds number ranging from 200 to 1000

Table 5.2 Results for Inclined fin Microchannel ($\theta = 45^0$)

S. No	Reynolds No	Outlet temperature	Heat transfer coefficient (h)	Pressure drop (ΔP)	COP
	-	K	W/m^{2}K	Pa	
1	200	310.34	17045.88	2100.46	8.12
2	400	305.17	22905.75	4814.76	4.76
3	600	303.45	28680.37	8151.17	3.52
4	800	302.59	33813.36	12319.8	2.74
5	1000	302.07	38143.68	16783.6	2.27

Table 5.3 Results for Inclined fin Microchannel ($\theta = 60^0$)

S. No	Reynolds No	Outlet temperature	Heat transfer coefficient (h)	Pressure drop (ΔP)	COP
	-	K	W/m^{2}K	Pa	
1	200	310.34	14101.84	2291.72	5.15
2	400	305.17	20313.53	5315.40	3.82
3	600	303.44	33941.35	9381.11	3.62
4	800	302.58	48159.44	16599.00	2.90
5	1000	302.07	52575.91	20855.60	2.52

Table 5.4 Results for Inclined fin Microchannel ($\theta = 90^0$)

S. No	Reynolds No	Outlet temperature	Heat transfer coefficient (h)	Pressure drop (ΔP)	COP
	-	K	W/m^{2}K	Pa	
1	200	310.34	15631.26	2517.91	5.21
2	400	305.17	33888.67	6383.14	5.31
3	600	303.45	58805.81	11679.60	5.04
4	800	302.57	69300.64	19259.60	3.60
5	1000	302.08	73291.78	28764.30	2.55

Table 5.5 Results for Inclined fin Microchannel ($\theta = 120^0$)

S. No	Reynolds No	Outlet temperature	Heat transfer coefficient (h)	Pressure drop (ΔP)	COP
	-	K	W/m^{2}K	Pa	
1	200	310.33	15180.07	2314.50	5.56
2	400	305.17	35185.29	5490.49	5.41
3	600	303.43	55772.89	10709.40	5.21
4	800	302.58	66712.19	16437.70	4.06
5	1000	302.07	68753.95	24102.60	2.85

Table 5.6 Results for Inclined fin Microchannel ($\theta = 150^0$)

S. No	Reynolds No	Outlet temperature	Heat transfer coefficient (h)	Pressure drop (ΔP)	COP
	-	K	W/m^{2}K	Pa	
1	200	318.15	10359.63	1865.69	5.55
2	400	314.07	17700.65	4042.76	4.38

S. No	Reynolds No	Outlet temperature	Heat transfer coefficient (h)	Pressure drop (ΔP)	COP
	-	K	W/m²K	Pa	
3	600	310.38	27285.03	6930.62	3.94
4	800	308.54	42113.62	11445.40	3.68
5	1000	307.43	47903.52	16285.00	2.94
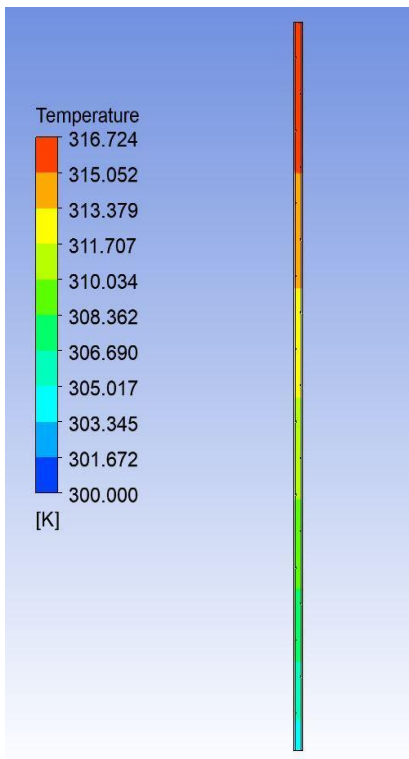
Fig 5.11 Temperature contour 45^0 Re=200
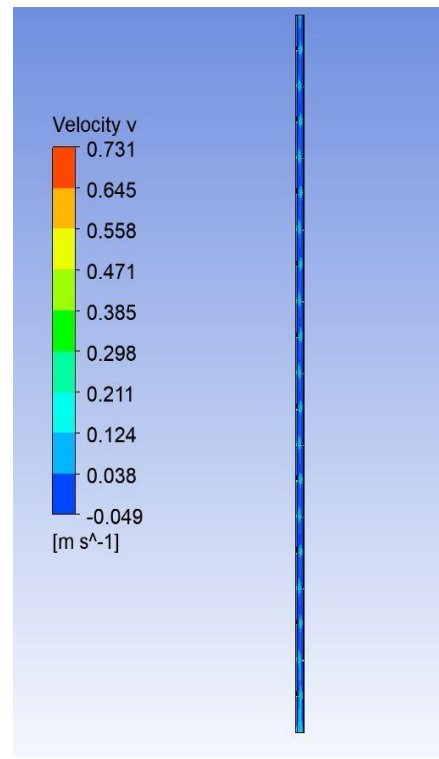
Fig 5.12 Velocity contour 45^0 Re=200
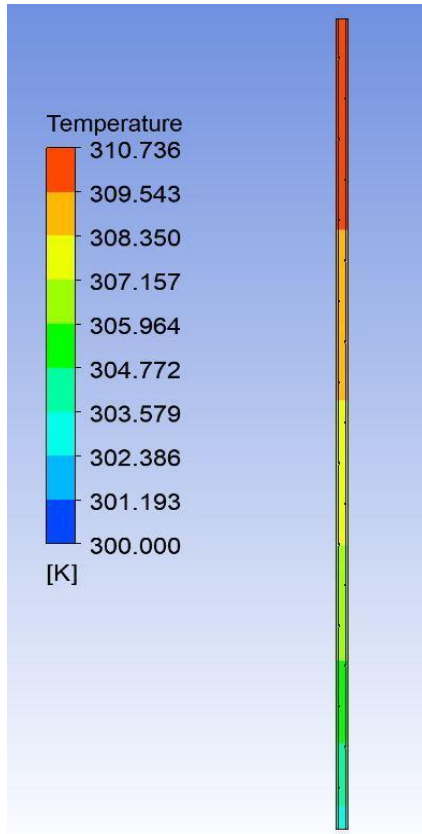
Fig 5.13 Temperature contour 45^0 Re=400
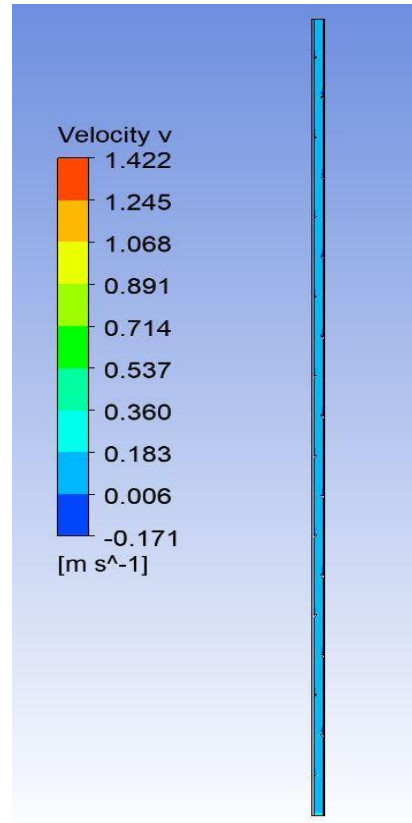
Fig 5.14 Velocity contour 45^0 Re=400
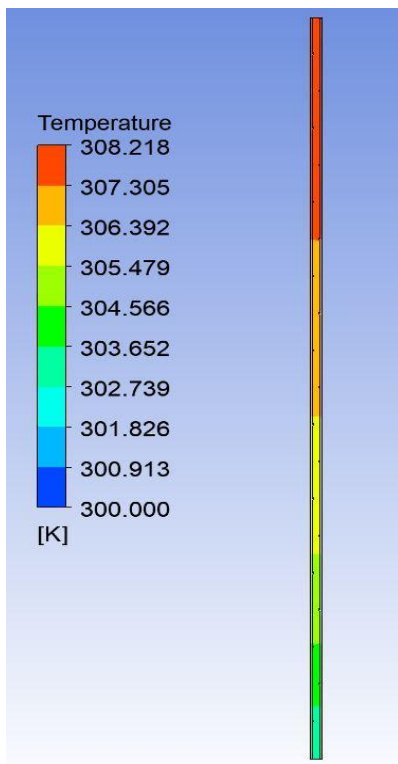
Fig 5.15 Temperature contour 45^0 Re=600
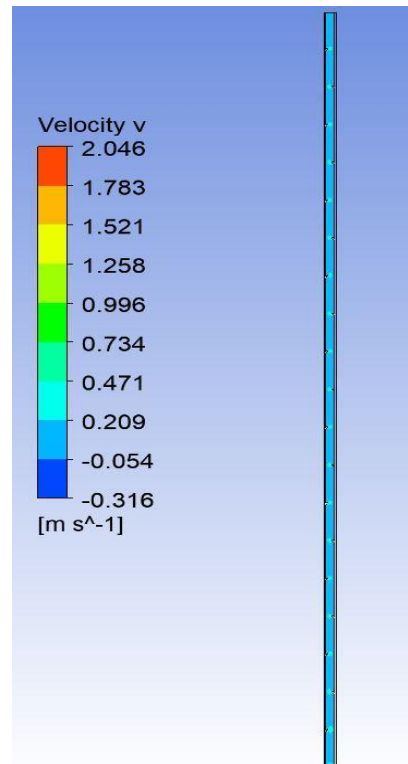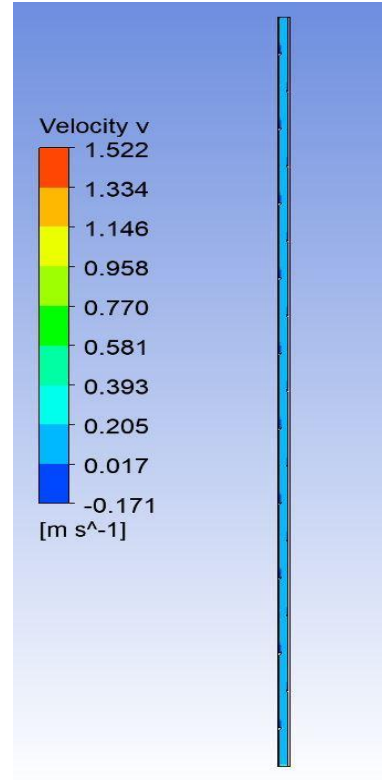

Fig 5.16 Velocity contour 45^0Re=600

27
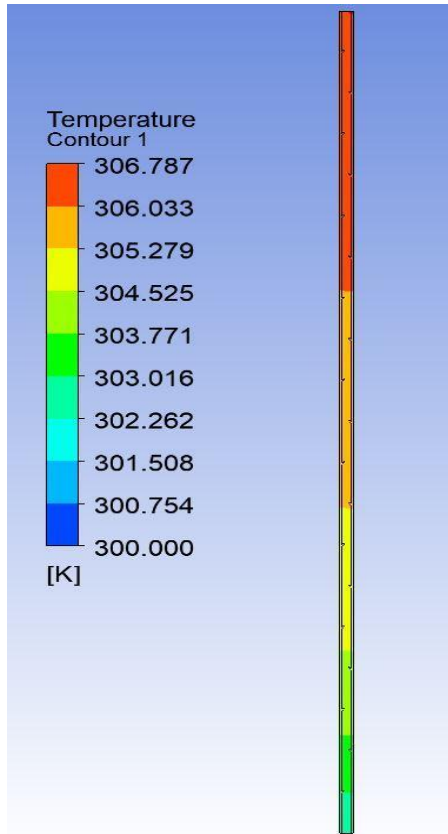
Fig 5.17 Temperature contour 45⁰ Re=800
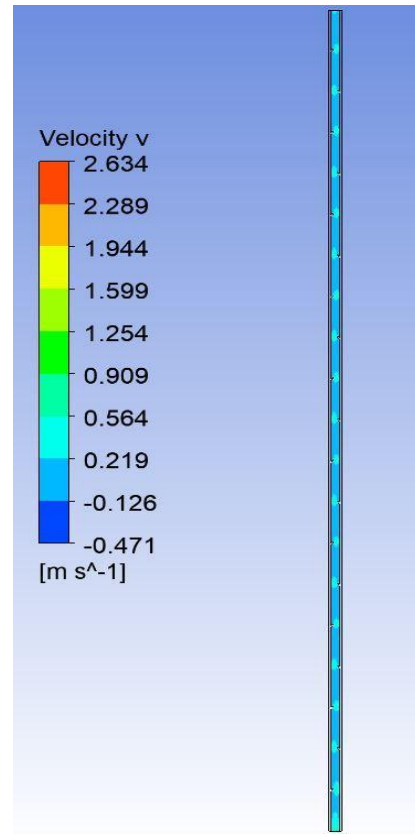
Fig 5.18 Velocity contour 45⁰ Re=800
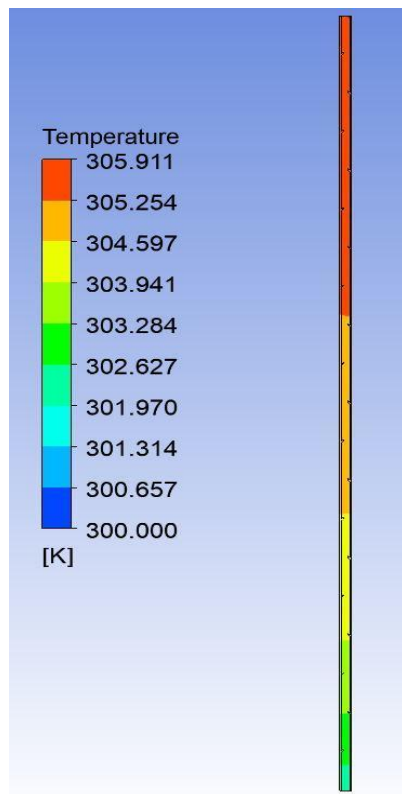
Fig 5.19 Temperature contour 45⁰ Re=1000
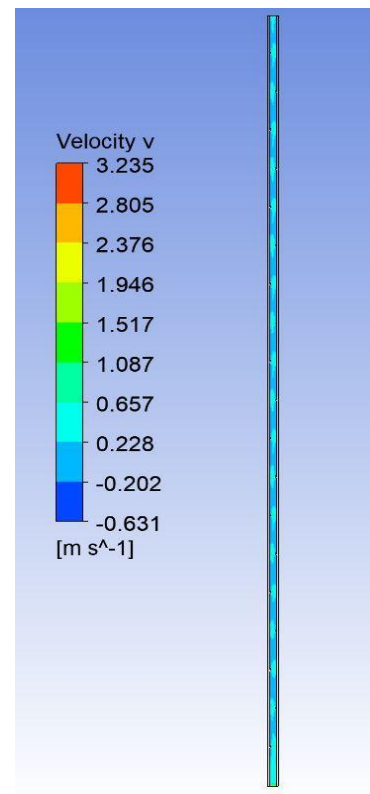
Fig 5.20 Velocity contour 45⁰Re=1000
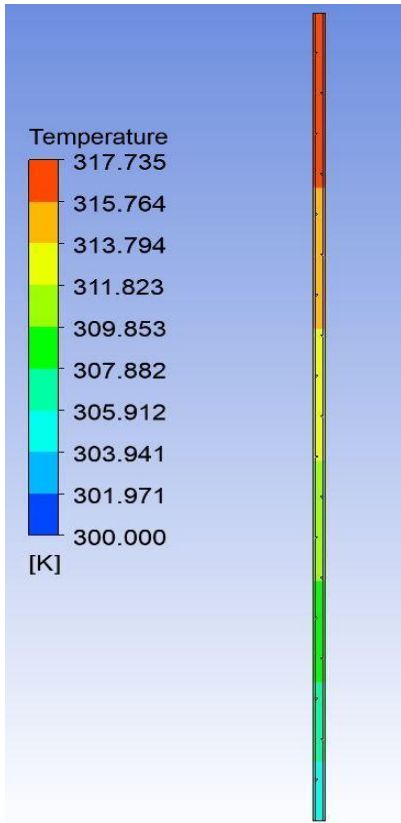
Fig 5.21 Temperature contour 60⁰ Re=200
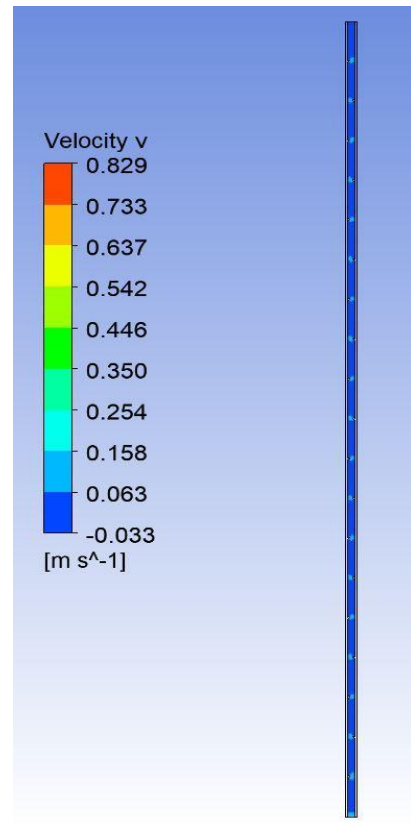
Fig 5.22 Velocity contour 60⁰ Re=200
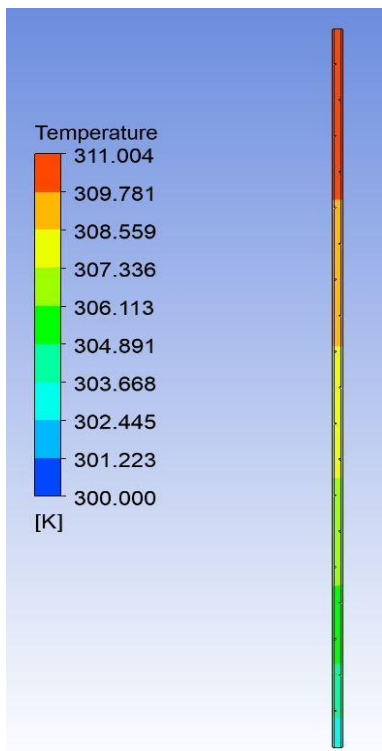
Fig 5.23 Temperature contour 60⁰ Re=400
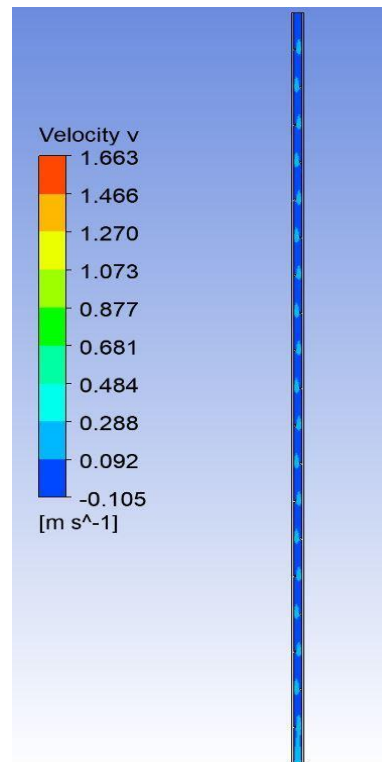
Fig 5.24 Velocity contour 60⁰ Re=400
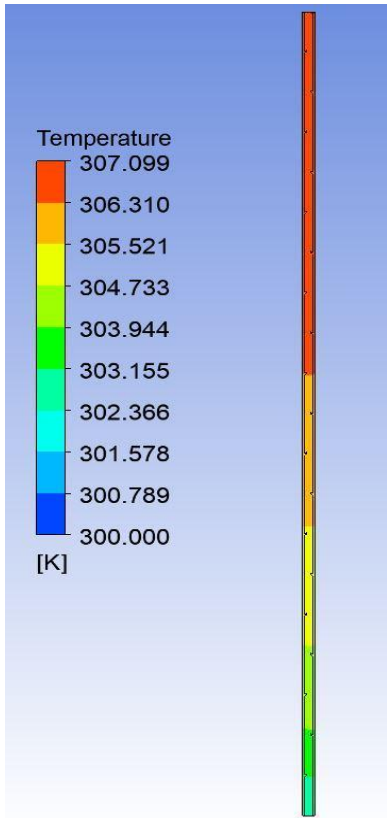
Fig 5.25 Temperature contour 60^0 Re=600
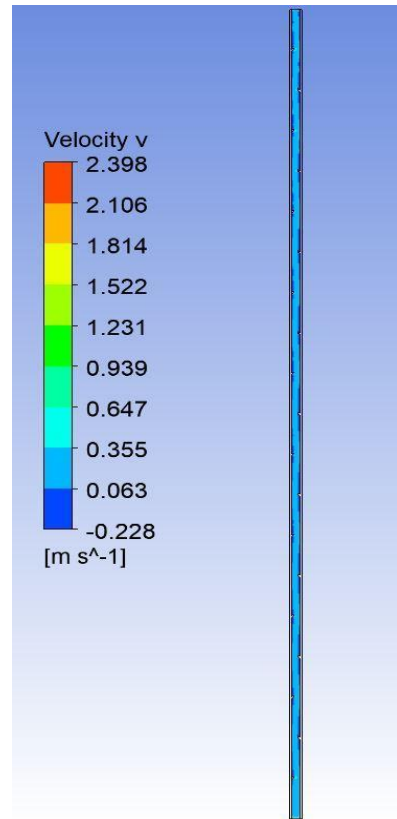
Fig 5.26 Velocity contour 60^0 Re=600
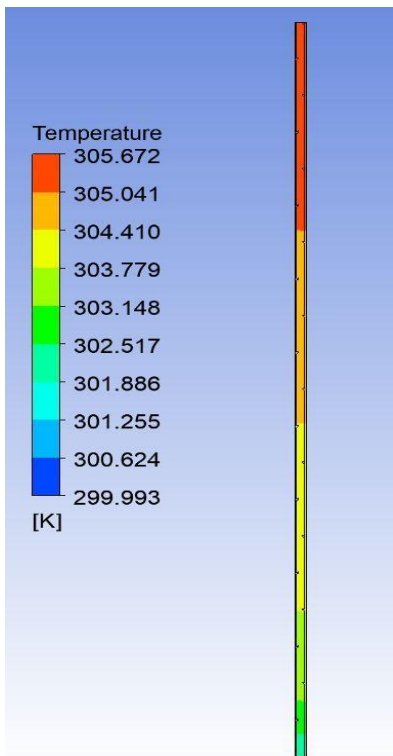
Fig 5.27 Temperature contour 60^0 Re=800
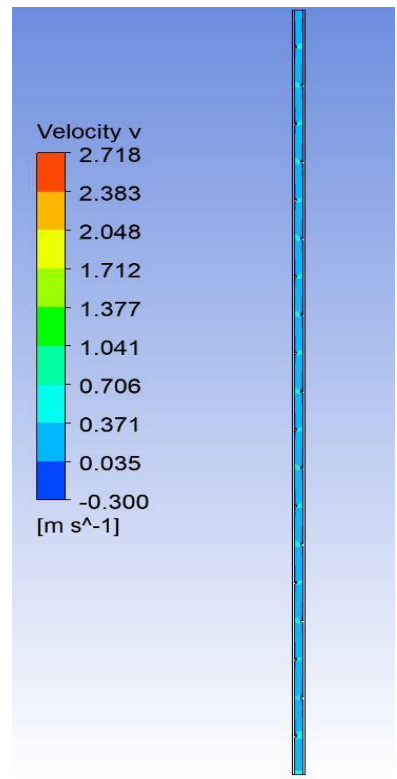
Fig 5.28 Velocity contour 60^0 Re=800
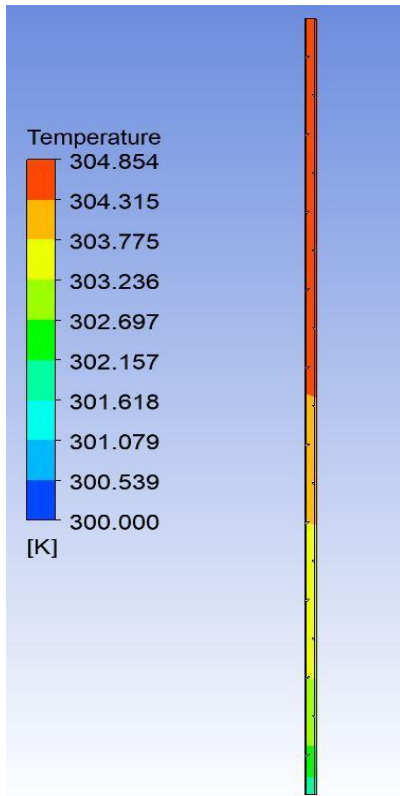
Fig 5.29 Temperature contour 60⁰ Re=1000
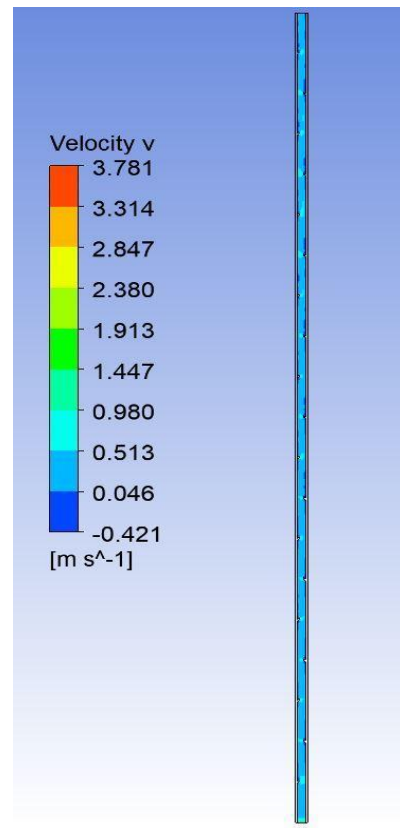
Fig 5.30 Velocity contour 60⁰ Re=1000
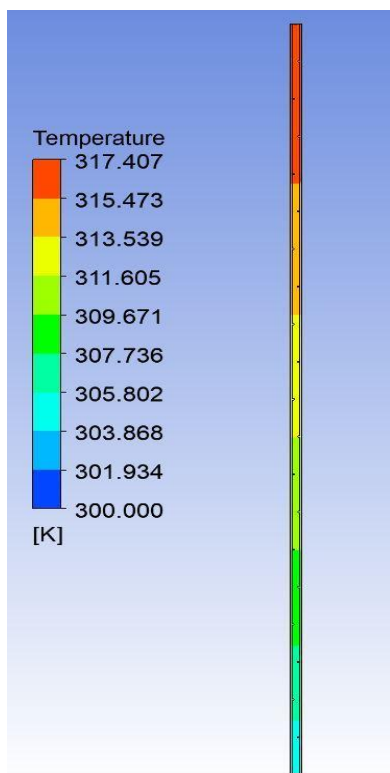
Fig 5.31 Temperature contour 90⁰ Re=200
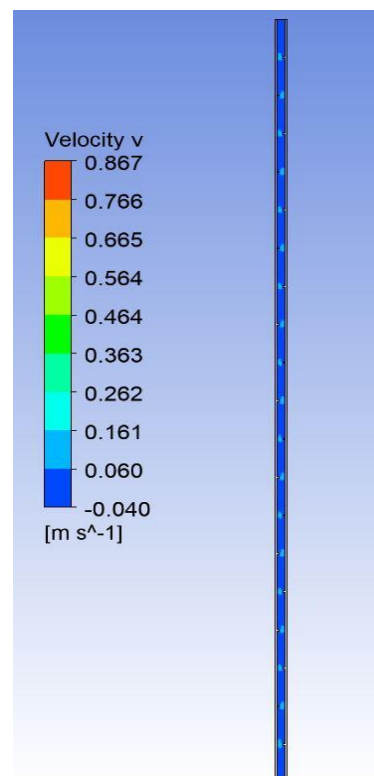
Fig 5.32 Velocity contour 90⁰ Re=200
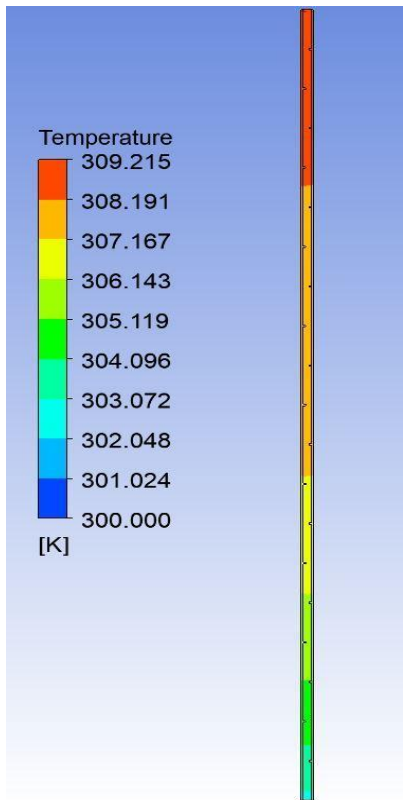
Fig 5.33 Temperature contour 90^0 Re=400
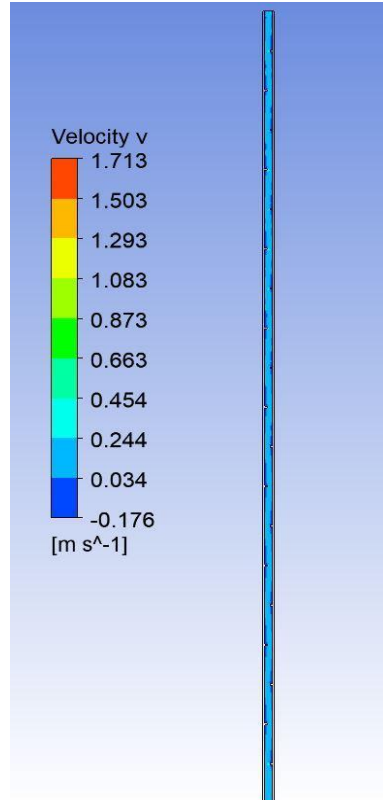
Fig 5.34 Velocity contour 90^0 Re=400
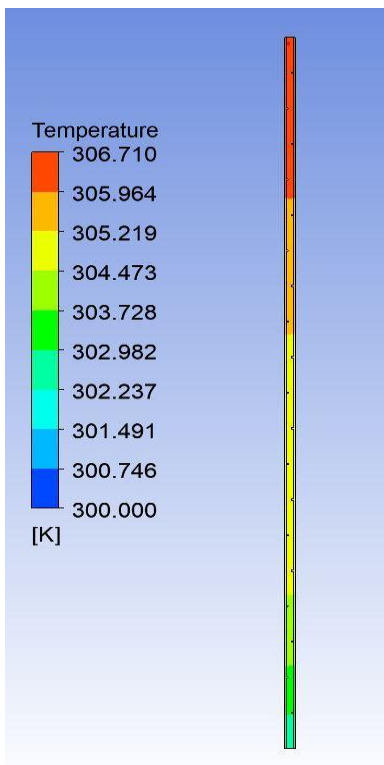

Fig 5.35 Temperature contour 90^0 Re=600
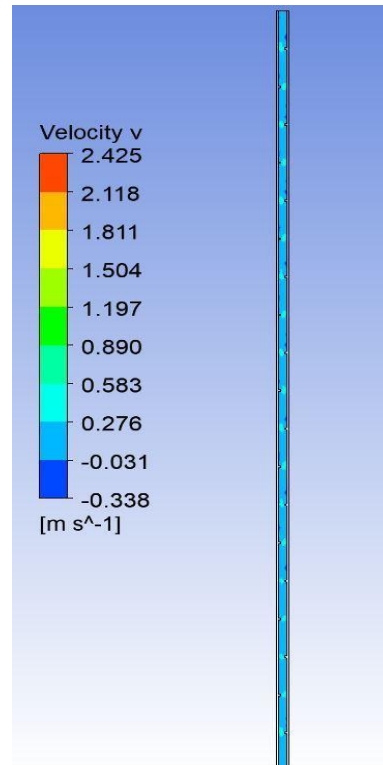
*Fig 5.36 Velocity contour 90^0 Re=600*
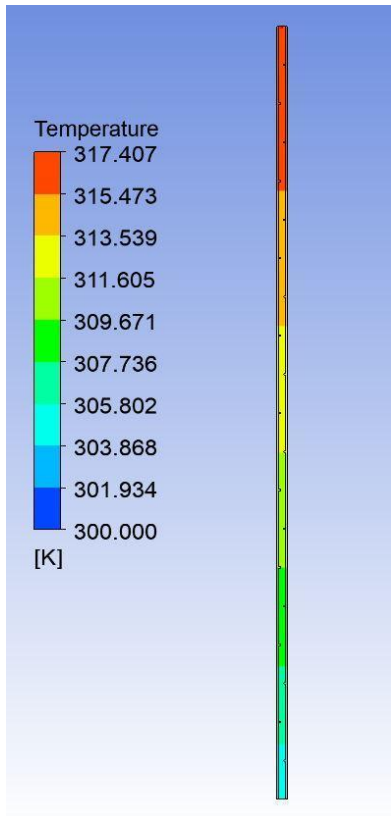
*Fig 5.37 Temperature contour 60^0 Re=800*
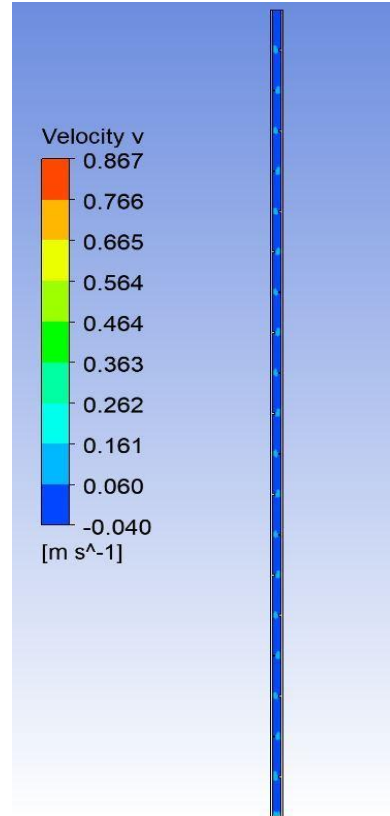
Fig 5.38 Velocity contour 60^0 Re=800
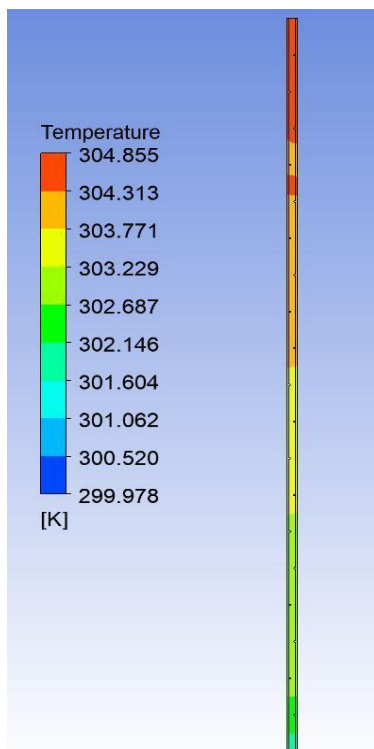
Fig 5.39 Temperature contour 90^0 Re=1000
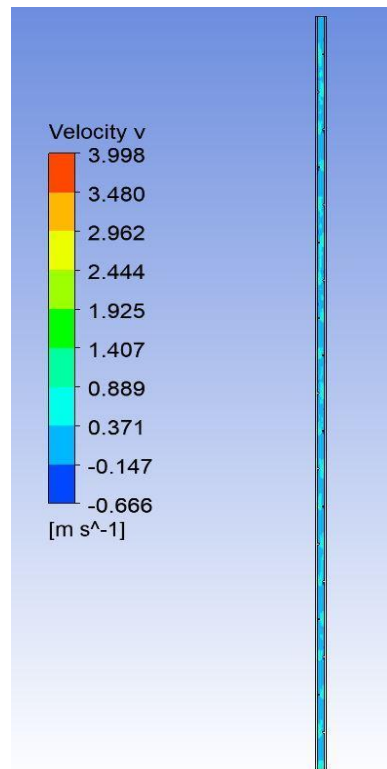
Fig 5.40 Velocity contour 90^0 Re=1000
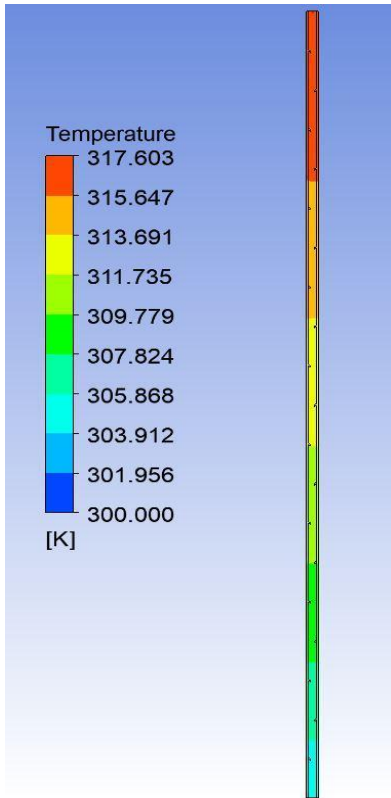
Fig 5.41 Temperature contour 120⁰ Re=200   ***Fig 5.42 Velocity contour 120⁰ Re=200***
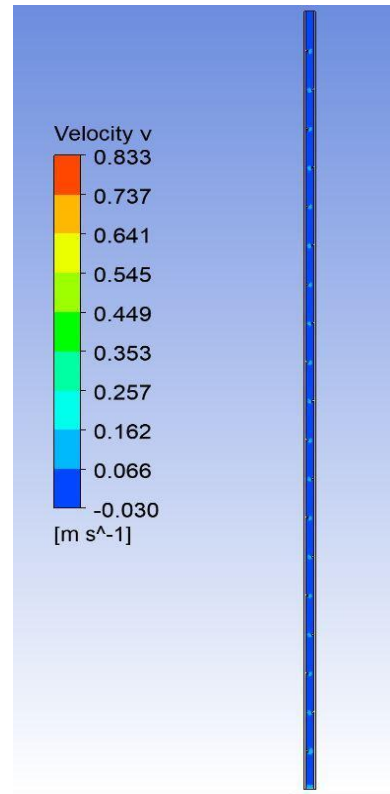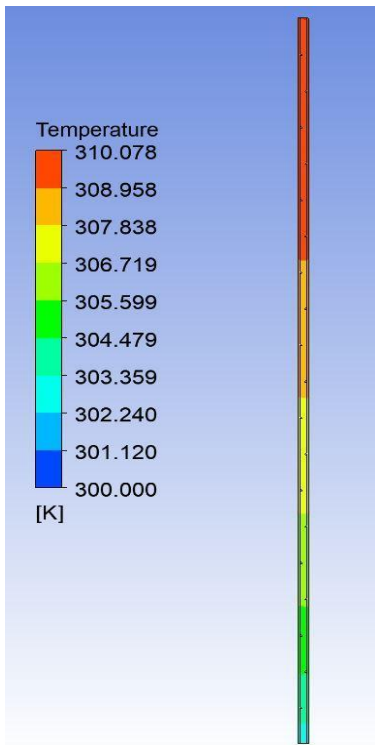
Fig 5.43 Temperature contour 120⁰ Re=400   ***Fig 5.44 Velocity contour 120⁰ Re=400***
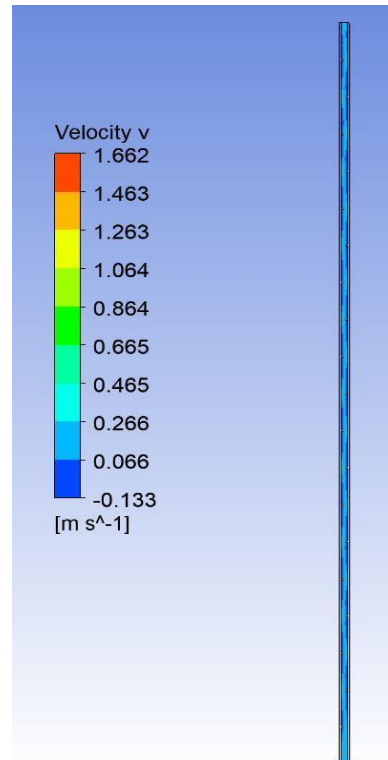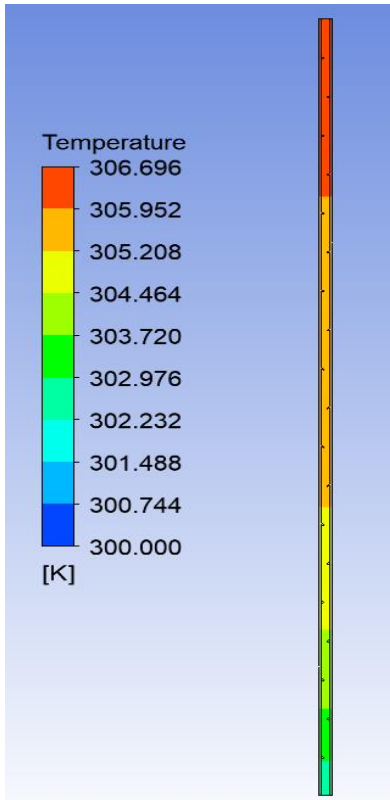
Fig 5.45 Temperature contour 120⁰ Re=600
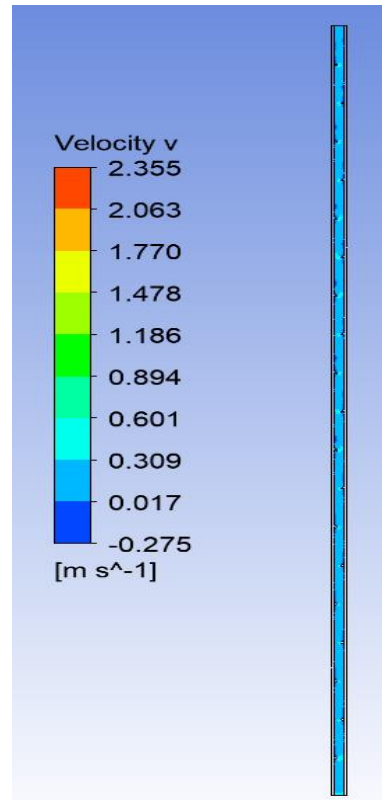
Fig 5.46 Velocity contour 120⁰ Re=600
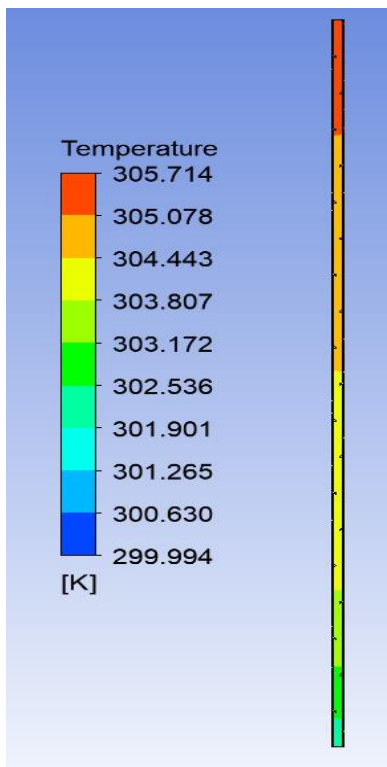
Fig 5.47 Temperature contour 120⁰ Re=800
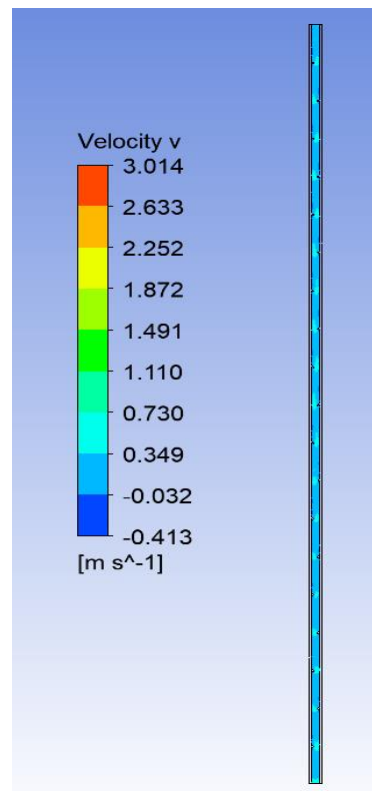
Fig 5.48 Velocity contour 120⁰ Re=800

35
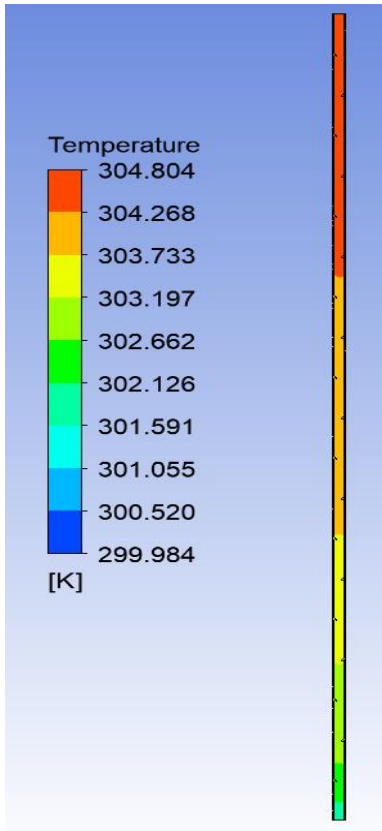
Fig 5.49 Temperature contour 120⁰ Re=1000
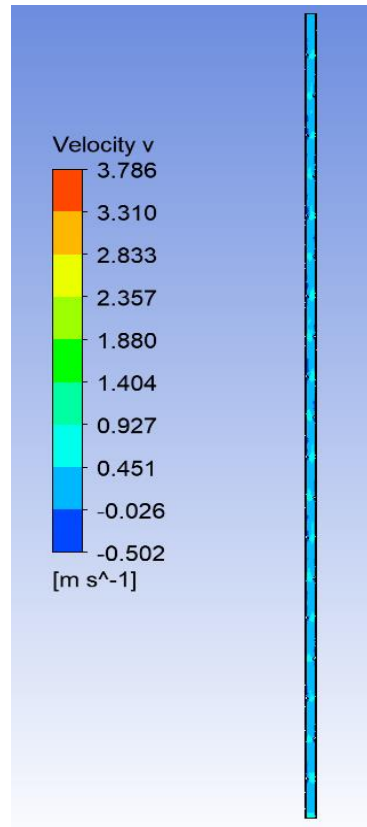
Fig 5.50 Velocity contour 120⁰ Re=1000
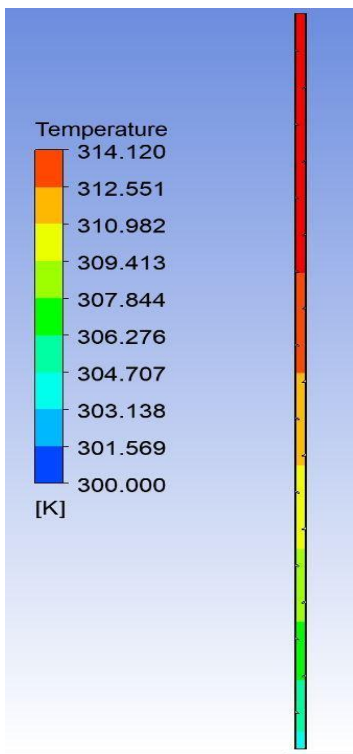
Fig 5.51 Temperature contour 150⁰ Re=200
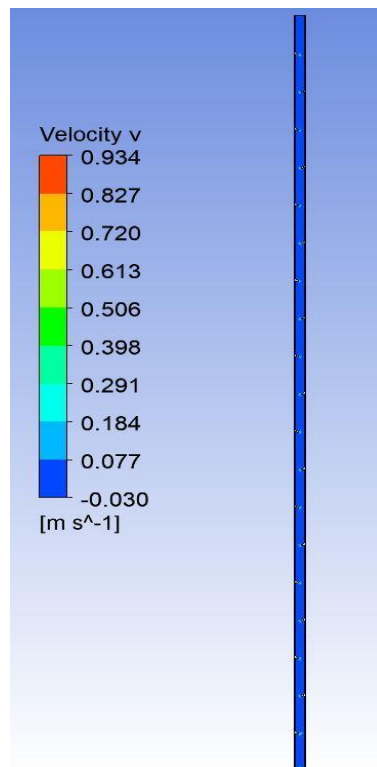
Fig 5.52 Velocity contour 150⁰ Re=200
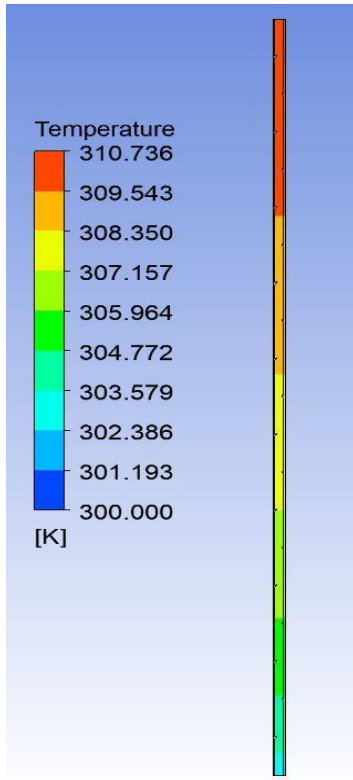
Fig 5.53 Temperature contour 150⁰ Re=400   ***Fig 5.54 Velocity contour 150⁰ Re=400***
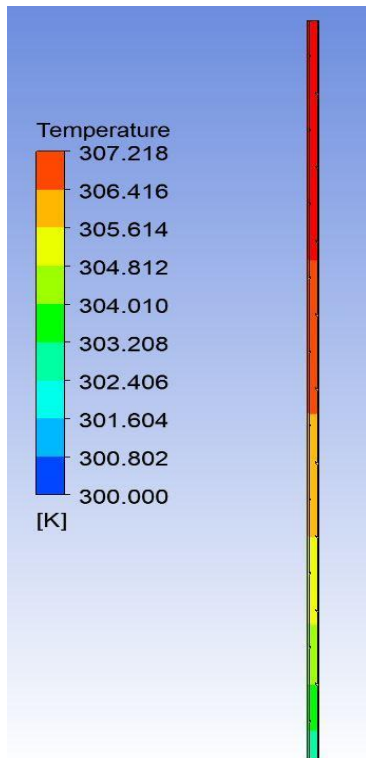
Fig 5.55 Temperature contour 150⁰ Re=600   ***Fig 5.56 Velocity contour 150 ⁰Re=600***
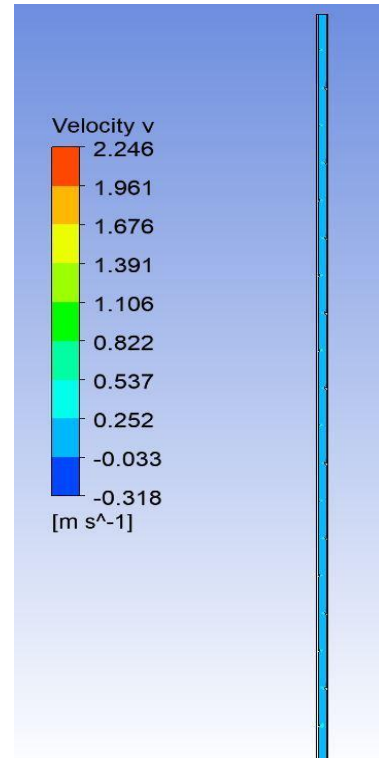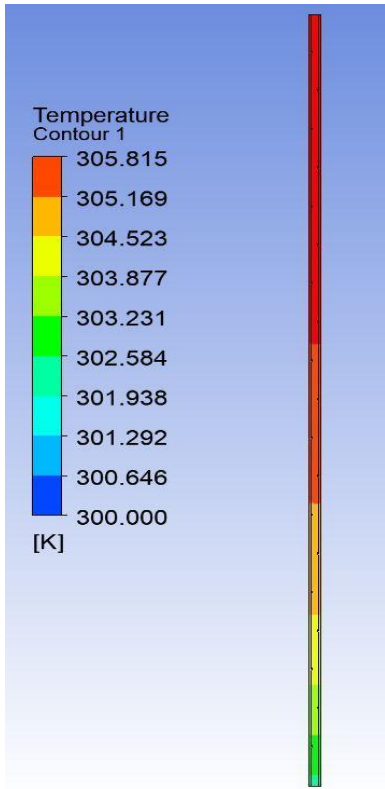
Fig 5.57 Temperature contour 150⁰ Re=800
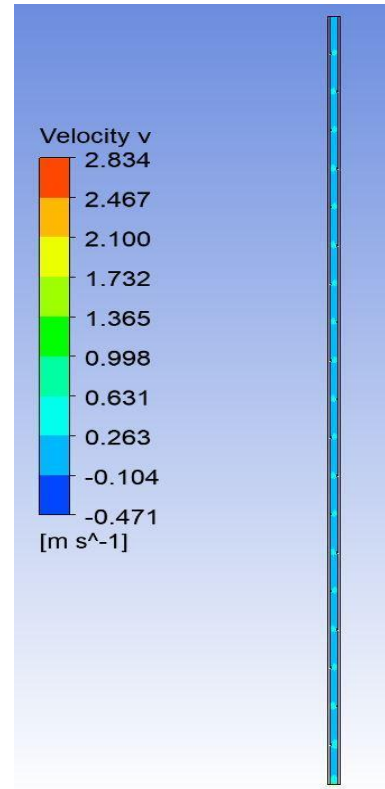
Fig 5.58 Velocity contour 150⁰ Re=800
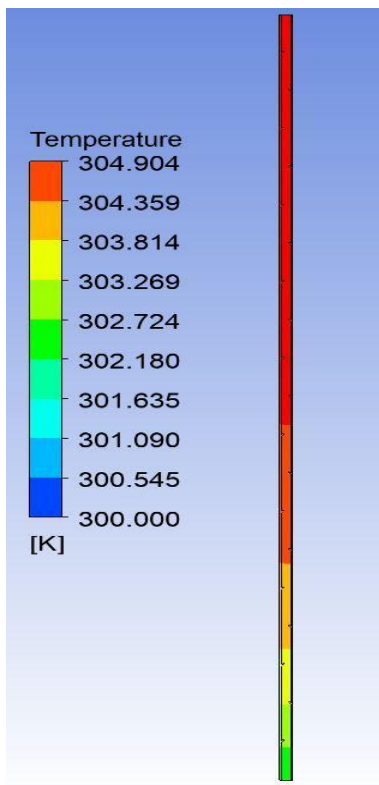
Fig 5.59 Temperature contour 150⁰Re=1000
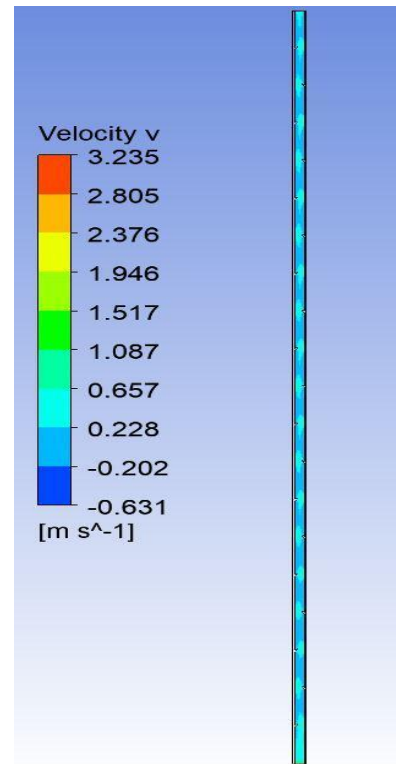
Fig 5.60 Velocity contour 150⁰Re=1000
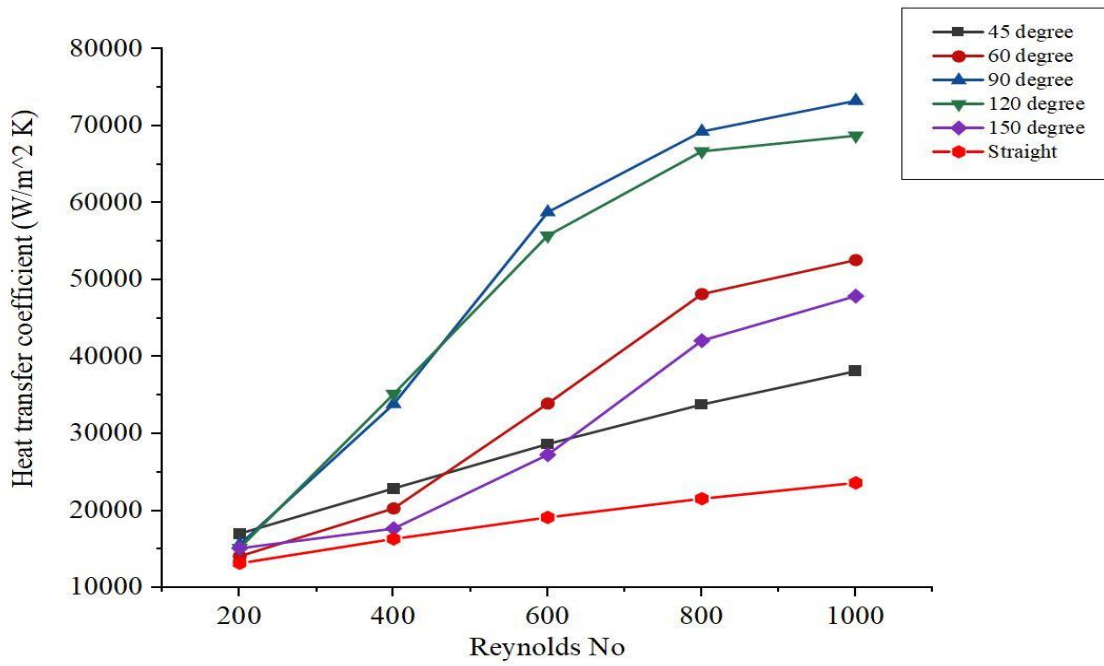
Fig 5.61 Graph for Inclined fin Channel (Heat transfer Coefficient Vs Reynolds No)
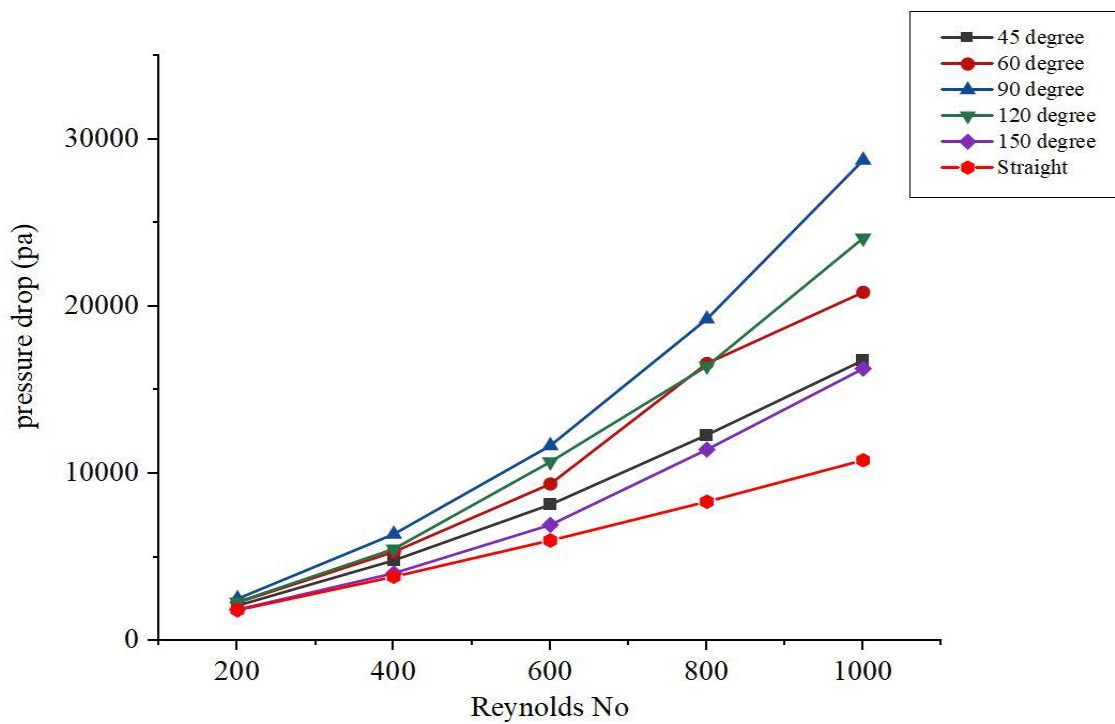
Fig 5.62 Graph for Inclined fin channel (Pressure drop Vs Reynolds No)
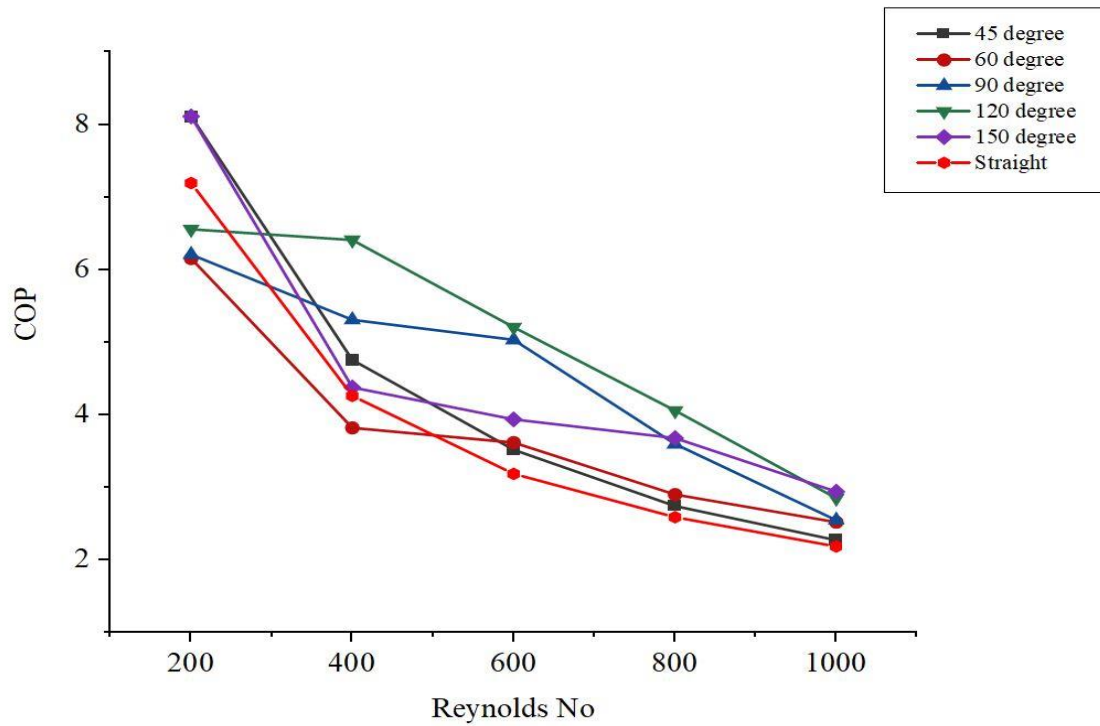
Fig 5.63 Graph for Inclined fin Channel (Coefficient of performance Vs Reynolds No)
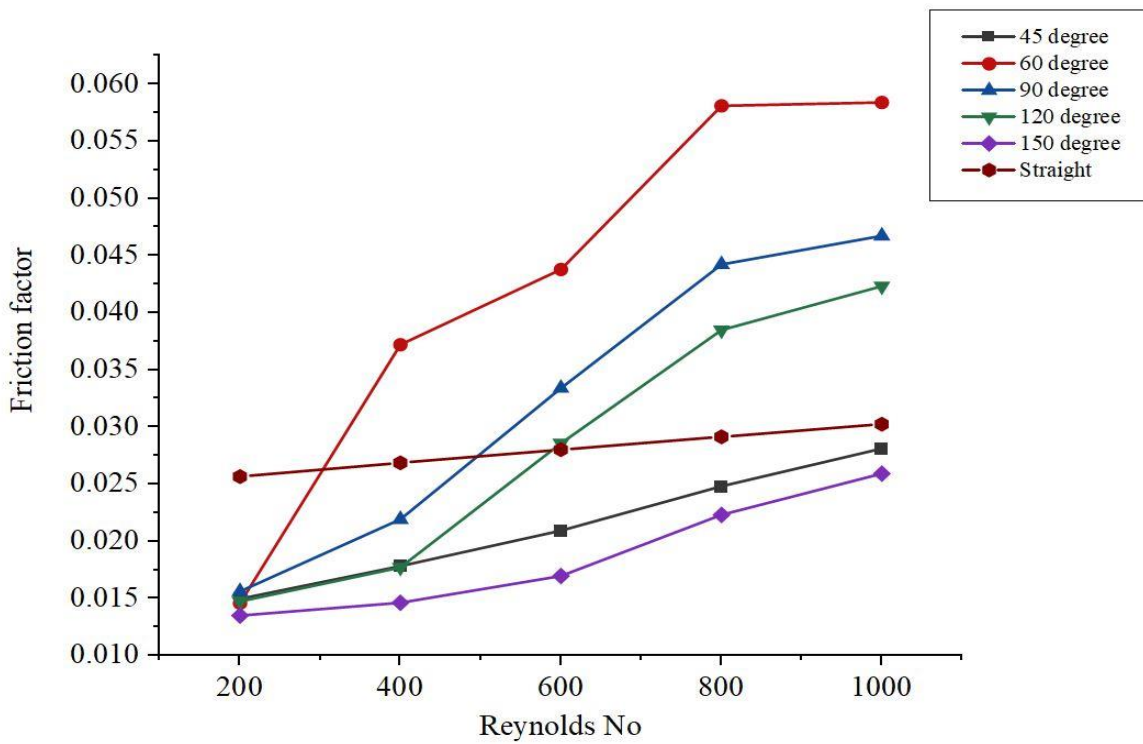
Fig 5.64 Graph for Inclined fin Channel (Friction factor Vs Reynolds No)

- As compared to the straight channel, Inclined channel possess higher Convective Heat transfer Coefficient and lower Pressure drop when the Reynolds number ranges between 400 to 600
- The coefficient of performance of the Inclined Microchannel is greater when the Reynolds number=200, more specifically for 45° and 150°
- The Friction factor value varies between 0.01 to 0.05 in all the cases.
- The Pumping power is higher in the case of 90° Microchannel at Re=1000
- On the whole, the Inclined channel 90° shows better results than other Inclined microchannel in terms of Heat transfer coefficient

<table>
<tr><td>

90° channel at Re = 400

h = 33888.67 W/m^2 K

ΔP = 6383.14 Pa

friction factor = 0.0219

COP = 5.3091

</td><td>

90° channel at Re = 600

h = 58806.81 W/m^2 K

ΔP =11679.60 Pa

friction factor = 0.0334

COP = 5.0350

</td></tr>
</table>

5.3 Ribbed Microchannel

In this type of Microchannel, Semi-circular section fin is introduced in the flow path of the microchannel which is oriented to the wall at 90 degrees. The heat transfer coefficient of this Microchannel is better than the Straight microchannel but not greater than Inclined fin Microchannel. Coefficient of performance is lesser than the straight microchannel because of the increase in pressure drop for higher Reynolds number.

As discussed earlier Ribbed fin is classified into Symmetric and Asymmetric type. The function parameters would be discussed in individual section.

5.3.1 Symmetric Ribbed Microchannel (SRC)

Table 5.7 Results for Symmetric Ribbed Microchannel (Rib Radius = 6mm)

S. No	Reynolds No	Outlet temperature	Heat transfer coefficient (h)	Pressure drop (ΔP)	COP
	-	K	W/m²K	Pa	
1	200	310.34	14105.84	3625.06	3.89
2	400	305.17	21955.81	8137.17	2.70
3	600	303.45	35818.94	14272.10	2.51
4	800	302.58	41928.43	22409.10	1.87
5	1000	302.06	49608.80	30448.80	1.63

Table 5.8 Results for Symmetric Ribbed Microchannel (Rib Radius = 7mm)

S. No	Reynolds No	Outlet temperature	Heat transfer coefficient (h)	Pressure drop (ΔP)	COP
	-	K	W/m²K	Pa	
1	200	310.34	12595.31	2635.59	4.78
2	400	305.17	16088.13	5732.61	2.81
3	600	303.45	19973.34	9194.46	2.17
4	800	302.59	23750.24	13154.20	1.81
5	1000	302.07	26643.18	17765.80	1.50

Table 5.9 Results for Symmetric Ribbed Microchannel (Rib Radius = 8mm)

S. No	Reynolds No	Outlet temperature	Heat transfer coefficient (h)	Pressure drop (ΔP)	COP
	-	K	W/m²K	Pa	
1	200	310.34	11940.84	2473.22	4.83
2	400	305.17	16681.79	5282.98	3.16
3	600	303.45	23287.89	8445.10	2.76

S. No	Reynolds No	Outlet temperature	Heat transfer coefficient (h)	Pressure drop (ΔP)	COP
	-	K	W/m²K	Pa	
4	800	302.59	28280.26	12020.30	2.35
5	1000	302.07	30765.44	16025.73	1.92

Figure 5.65 to 5.124 shows the temperature and velocity contours for the Ribbed fin microchannels for the Reynolds number ranging from 200 to 1000.

5.3.2 Asymmetric Ribbed Microchannel (ARC)

Table 5.10 Results for Asymmetric Ribbed Microchannel (Rib Radius = 6mm)

S. No	Reynolds No	Outlet temperature	Heat transfer coefficient (h)	Pressure drop (ΔP)	COP
	-	K	W/m²K	Pa	
1	200	310.34	14615.55	2912.53	5.02
2	400	305.17	21969.40	6392.73	3.44
3	600	303.45	29752.35	10518.80	2.83
4	800	302.58	35285.75	15351.20	2.30
5	1000	302.06	40458.76	20995.6	1.92

Table 5.11 Results for Asymmetric Ribbed Microchannel (Rib Radius = 7mm)

S. No	Reynolds No	Outlet temperature	Heat transfer coefficient (h)	Pressure drop (ΔP)	COP
	-	K	W/m²K	Pa	
1	200	310.34	14530.03	2635.16	5.51

S. No	Reynolds No	Outlet temperature	Heat transfer coefficient (h)	Pressure drop (ΔP)	COP
	-	K	W/m^{2}K	Pa	
2	400	305.17	19365.20	5734.13	3.38
3	600	303.45	25325.40	9193.30	2.75
4	800	302.59	31615.51	13152.80	2.40
5	1000	302.07	36965.93	17769.60	2.08

Table 5.12 Results for Asymmetric Ribbed Microchannel (Rib Radius = 8mm)

S. No	Reynolds No	Outlet temperature	Heat transfer coefficient (h)	Pressure drop (ΔP)	COP
	-	K	W/m^{2}K	Pa	
1	200	310.34	14207.78	2467.16	5.76
2	400	305.17	18655.86	5275.98	3.54
3	600	303.45	23249.21	8439.10	2.75
4	800	302.59	28084.37	12007.30	2.34
5	1000	302.07	32609.64	16015.70	2.04
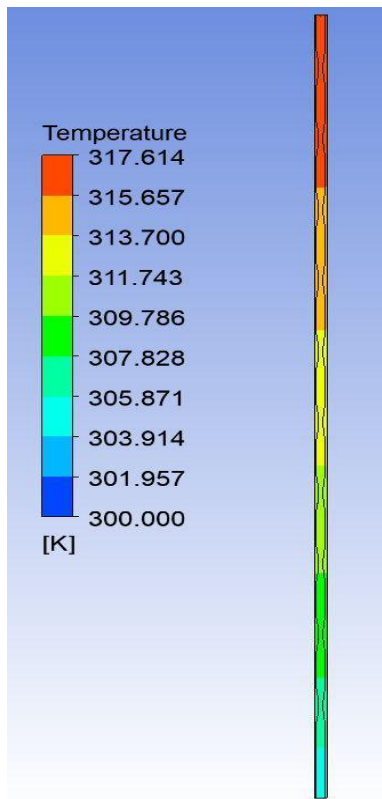
Fig 5.65 Temperature contour SRC6mm Re=200   *Fig 5.66 Velocity contour SRC6mm Re=200*
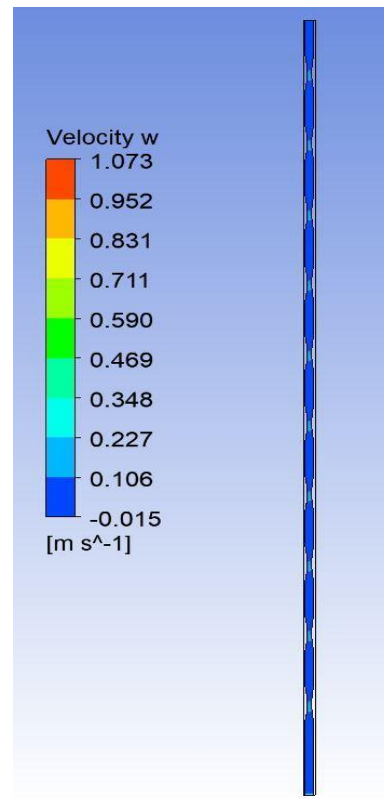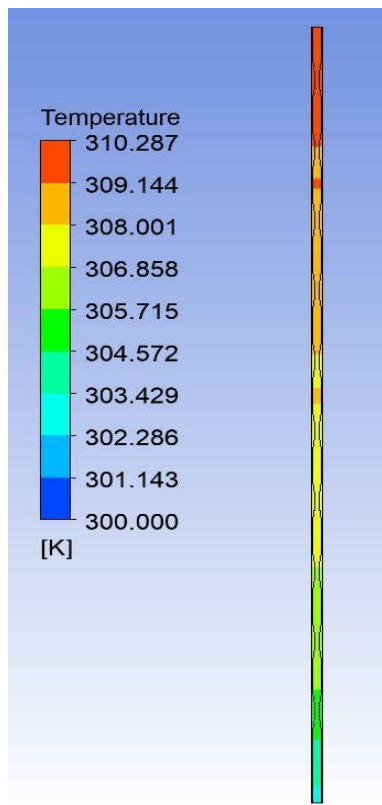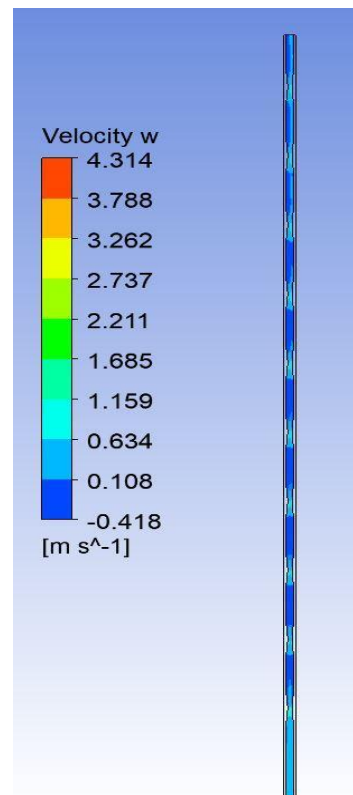

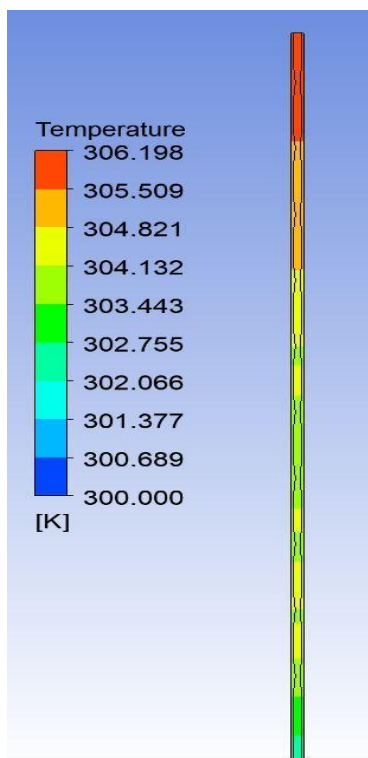*Fig 5.67 Temperature contour SRC6mm Re=400*   *Fig 5.68 Velocity contour SRC6mm Re=400*
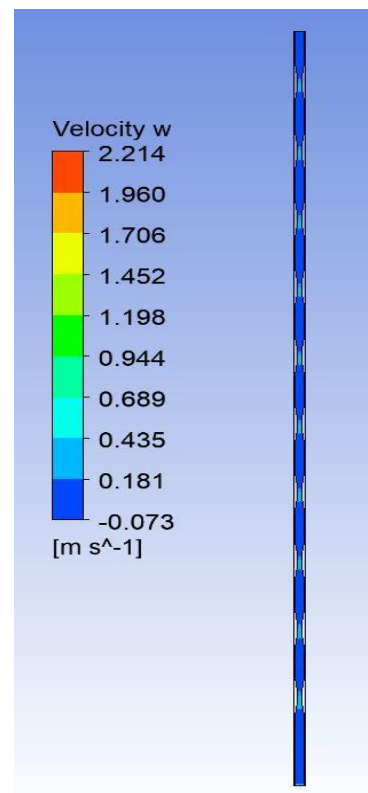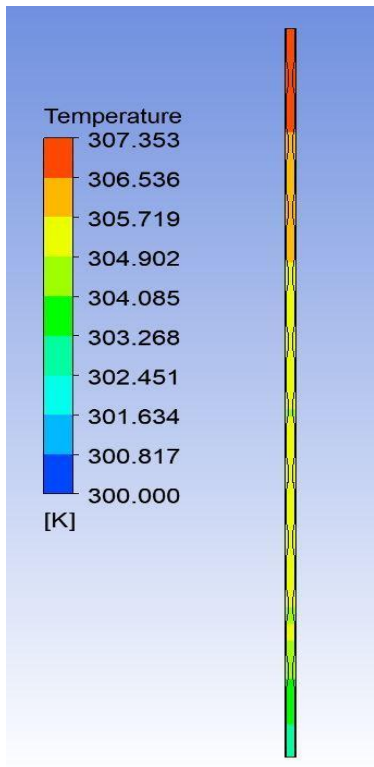
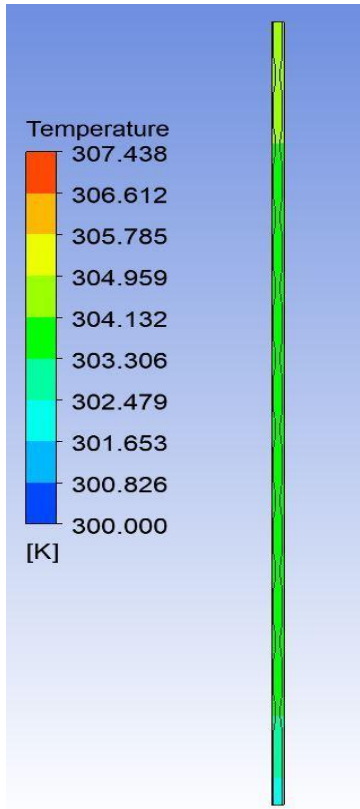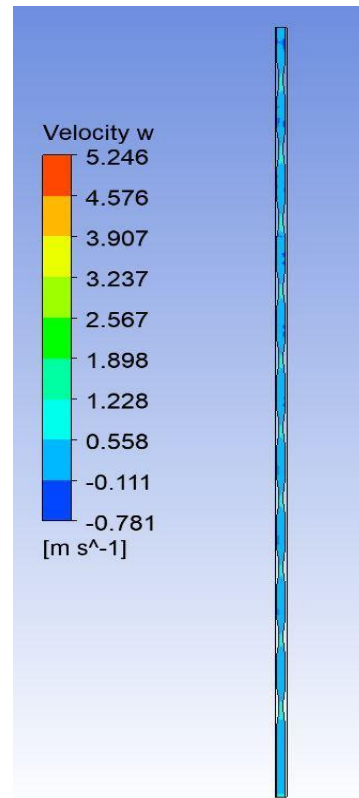*Fig 5.69 Temperature contour SRC6mm Re=600*
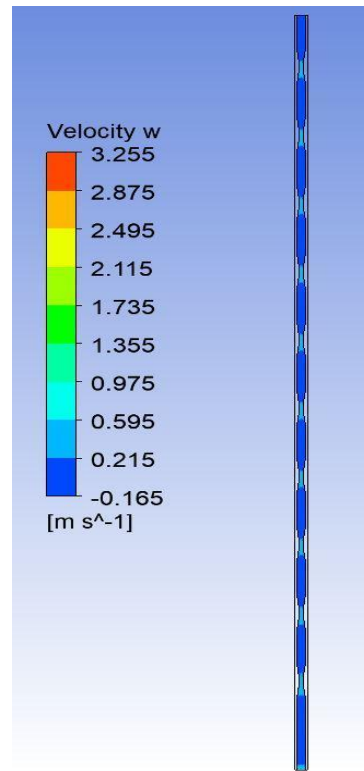
Fig 5.70 Velocity contour SRC6mm Re=600
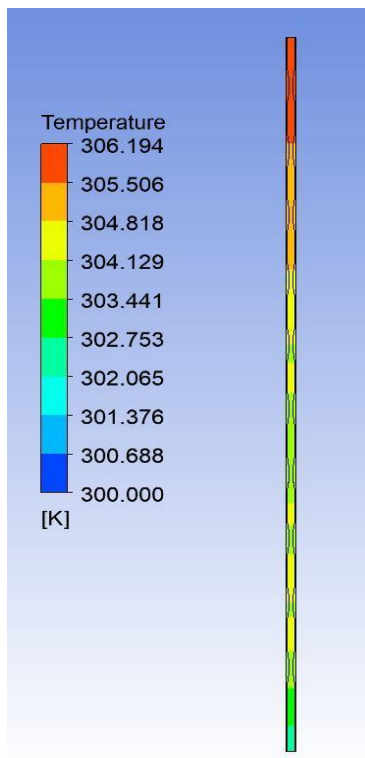
Fig 5.71 Temperature contour SRC6mm Re=800
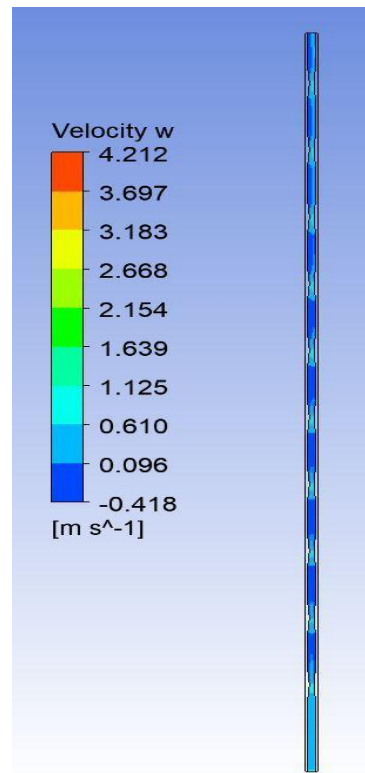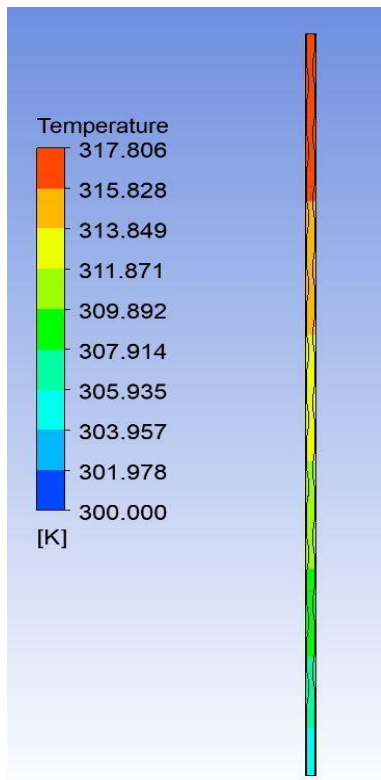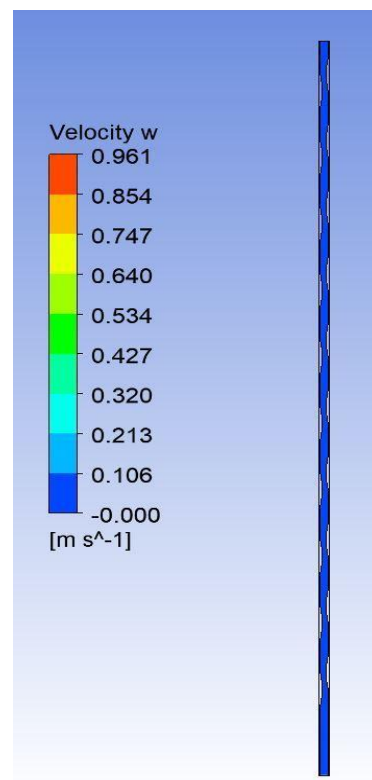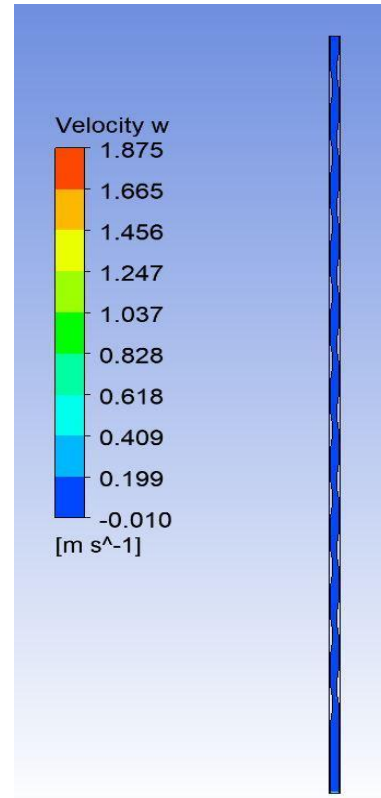

Fig 5.72 Velocity contour SRC6mm Re=800
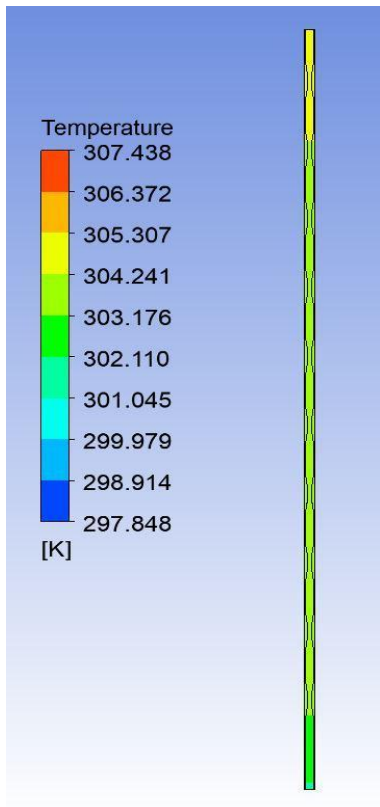
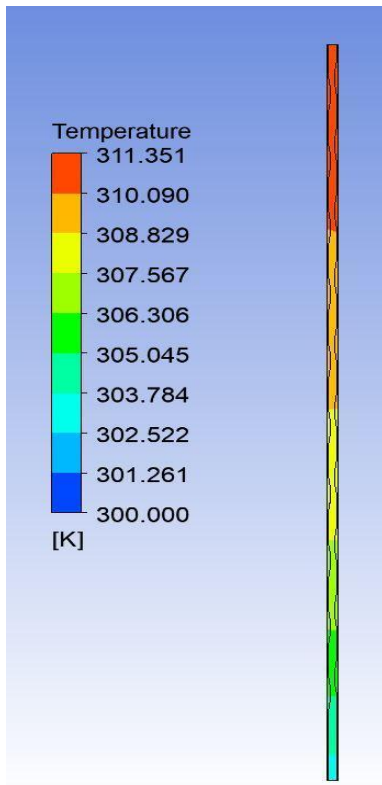*Fig 5.73 Temperature contour SRC6mm Re=1000*   *Fig 5.74 Velocity contour SRC6mm Re=1000*
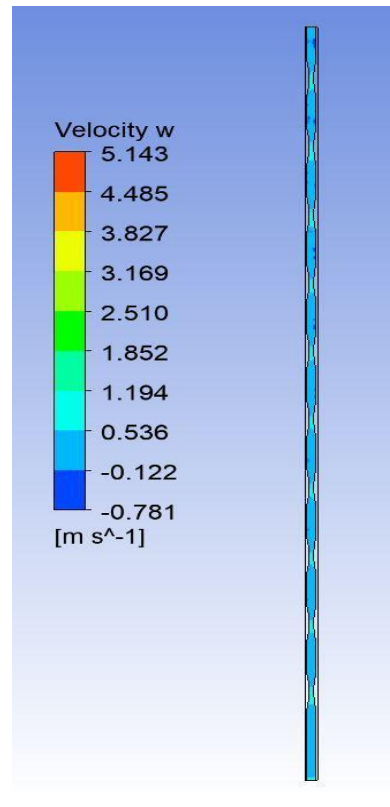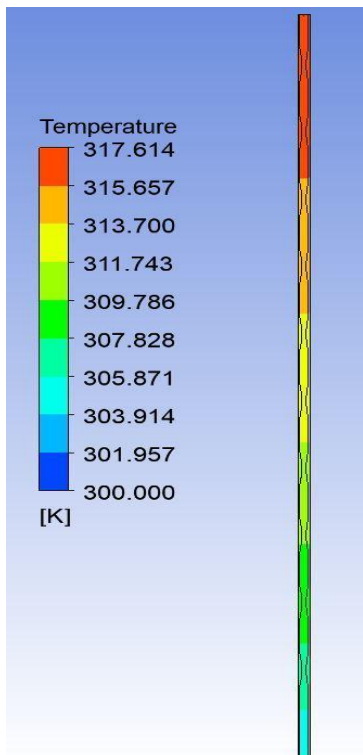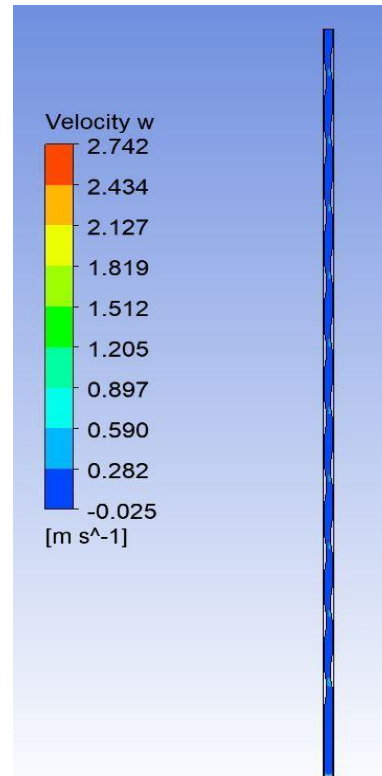

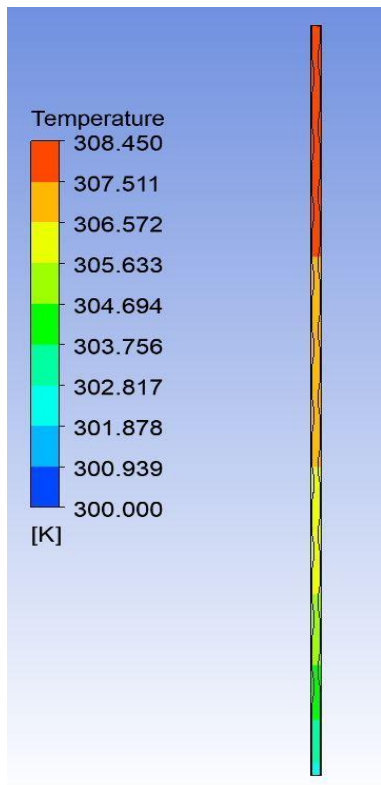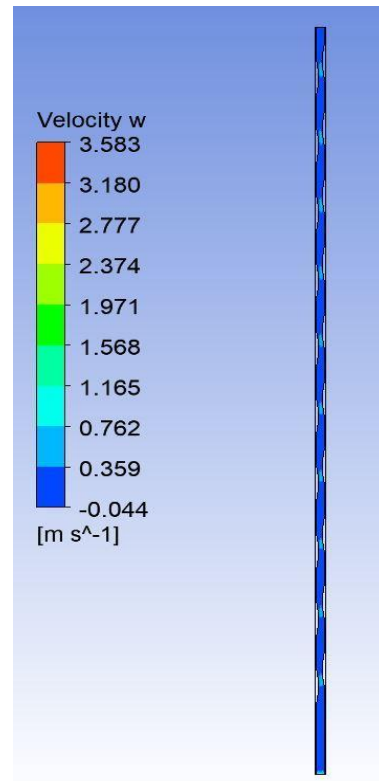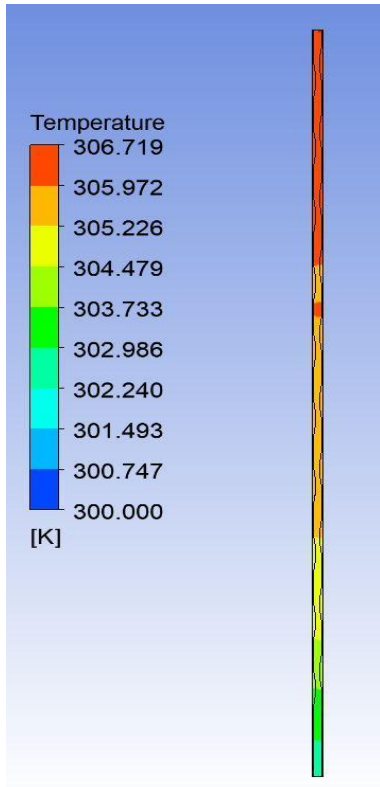*Fig 5.75 Temperature contour SRC7mm Re=200*   *Fig 5.76 Velocity contour SRC7mm Re=200*
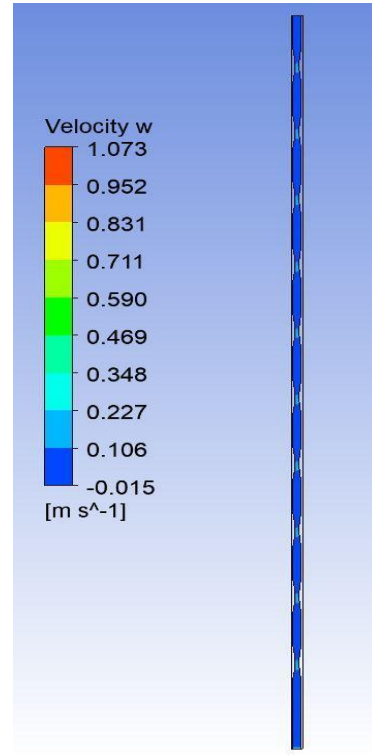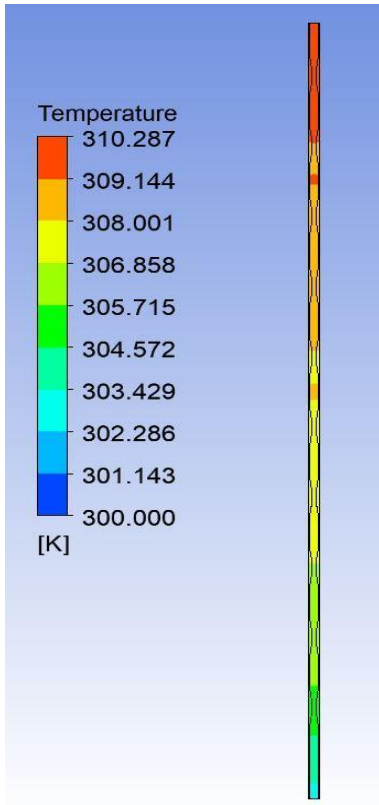
Fig 5.77 Temperature contour SRC7mm Re=400
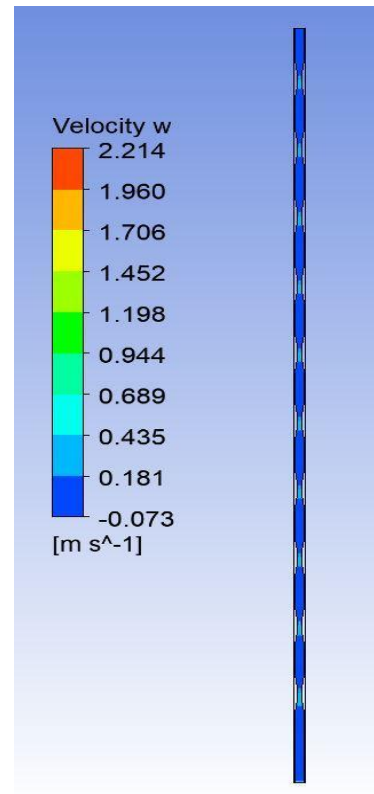
Fig 5.78 Velocity contour SRC7mm Re=400
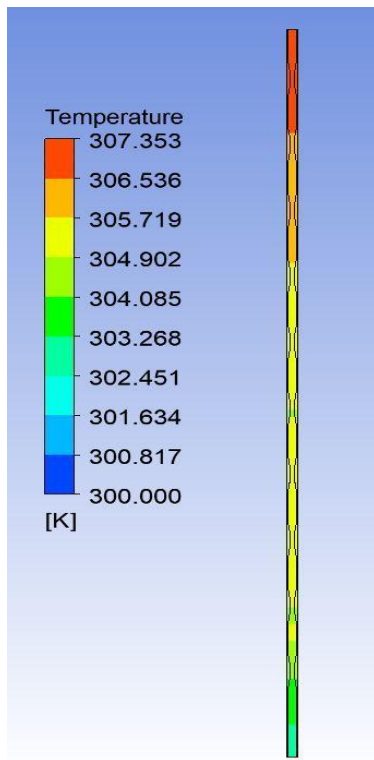
Fig 5.79 Temperature contour SRC7mm Re=600
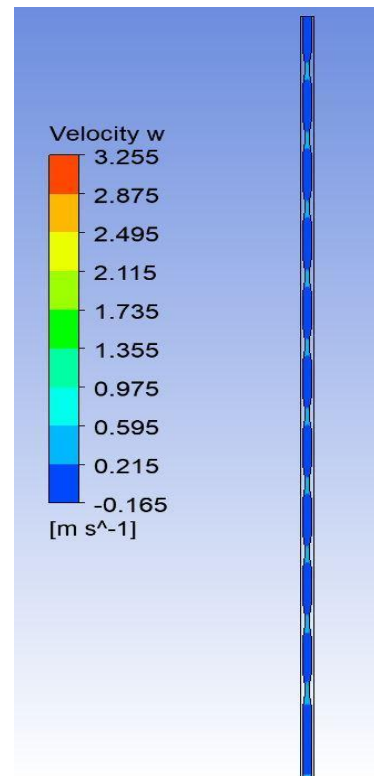
Fig 5.80 Velocity contour SRC7mm Re=600
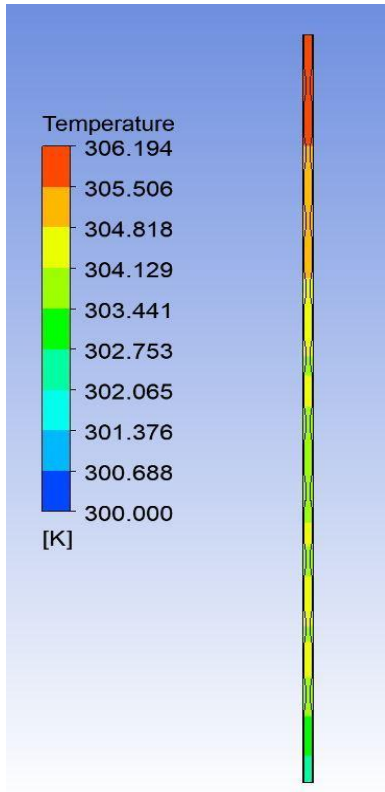
Fig 5.81 Temperature contour SRC7mm Re=800
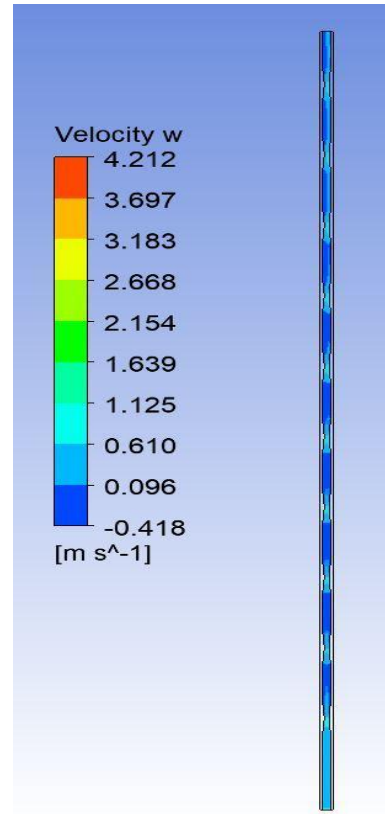
Fig 5.82 Velocity contour SRC6mm Re=800
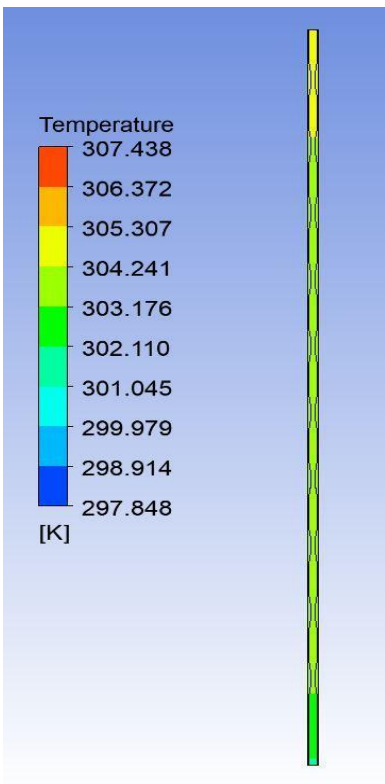
Fig 5.83 Temperature contour SRC7mm Re=1000
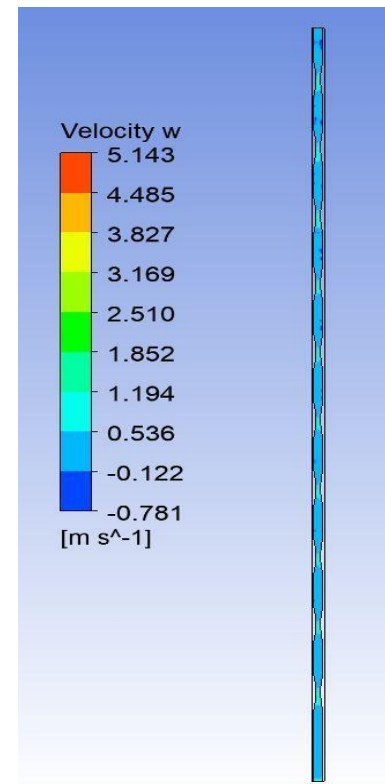
Fig 5.84 Velocity contour SRC7mm Re=1000
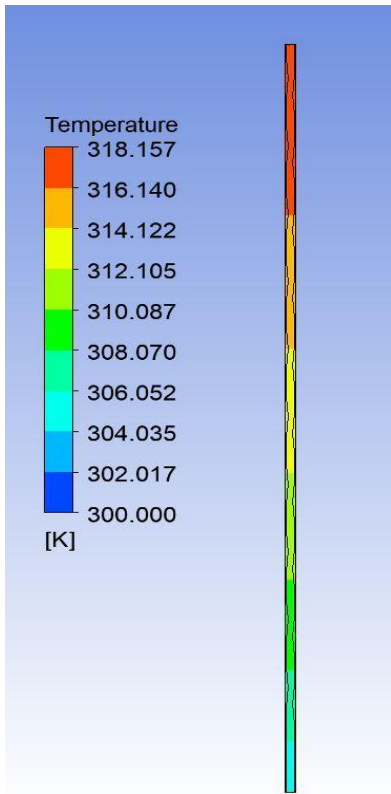
Fig 5.85 Temperature contour SRC8mm Re=200   *Fig 5.86 Velocity contour SRC8mm Re=200*
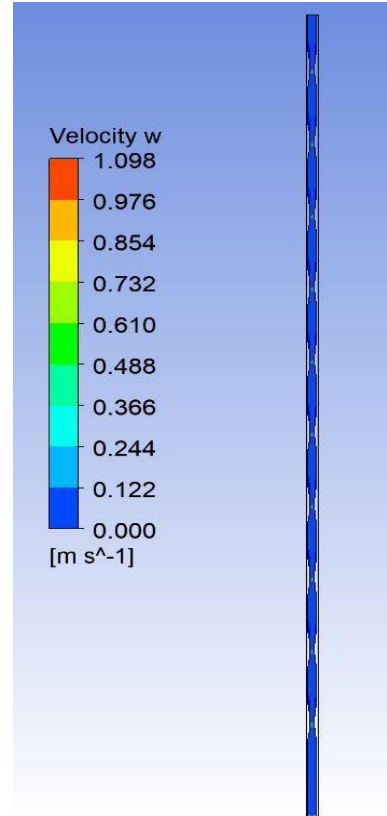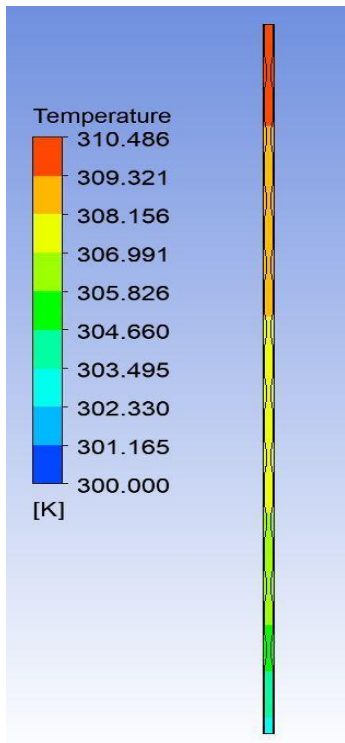
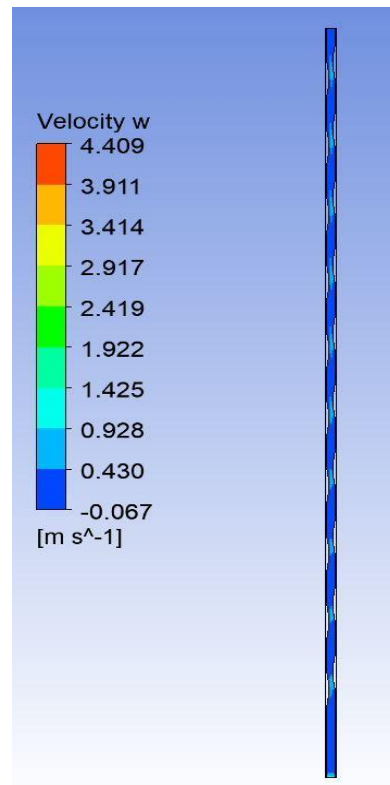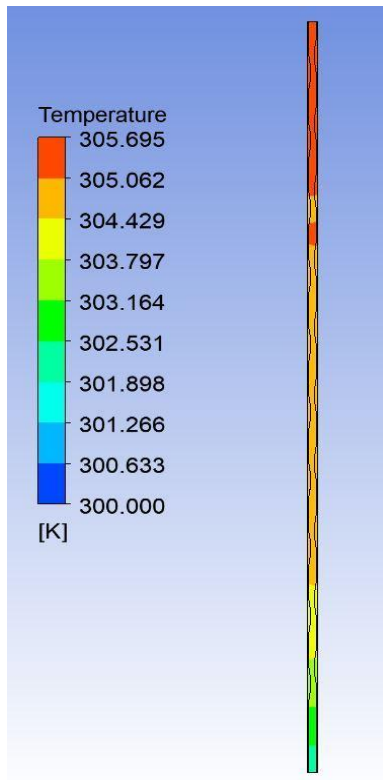*Fig 5.87 Temperature contour SRC8mm Re=400*   *Fig 5.88 Velocity contour SRC8mm Re=400*
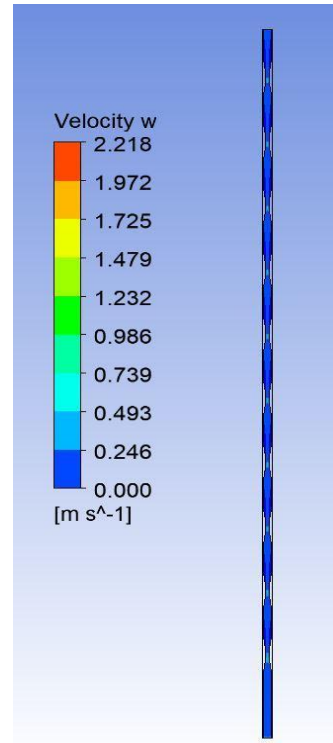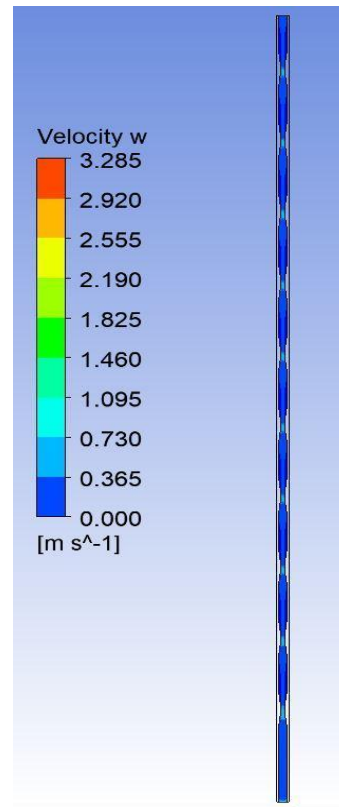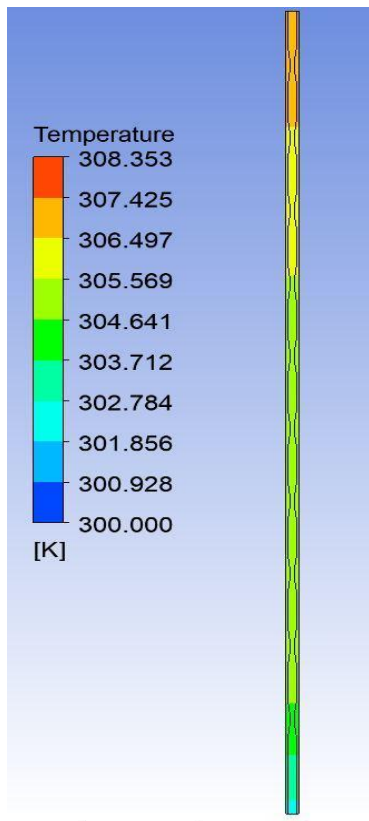
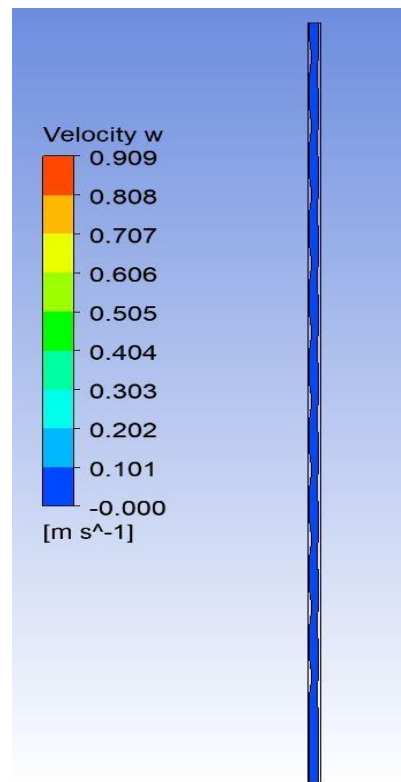*Fig 5.89 Temperature contour SRC8mm Re=600*   *Fig 5.90 Velocity contour SRC8mm Re=60*

Fig 5.91 Temperature contour SRC8mm Re=800   *Fig 5.92 Velocity contour SRC8mm Re=200*

Fig 5.93 Temperature contour SRC8mm Re=1000   *Fig 5.94 Velocity contour SRC8mm Re=1000*

Fig 5.95 Temperature contour ARC6mm Re=200   *Fig 5.96 Velocity contour ARC6mm Re=200*

Fig 5.97 Temperature contour ARC 6mm Re=400   ***Fig 5.98 Velocity contour ARC 6mmRe=400***

Fig 5.99 Temperature contour ARC6mm Re=600   **Fig 5.100 Velocity contour ARC6mm Re=600**
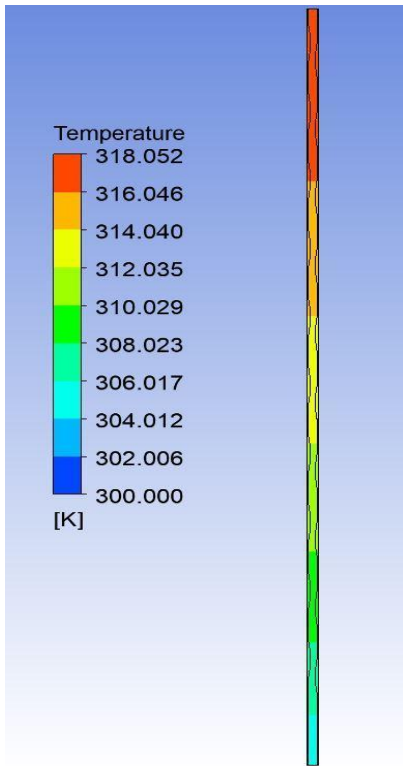
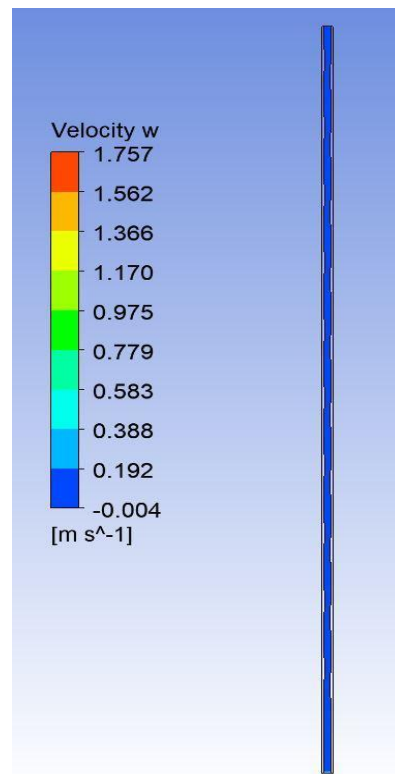*Fig 5.101 Temperature contour ARC6mm Re=800*   *Fig 5.102 Velocity contour ARC6mm Re=800*
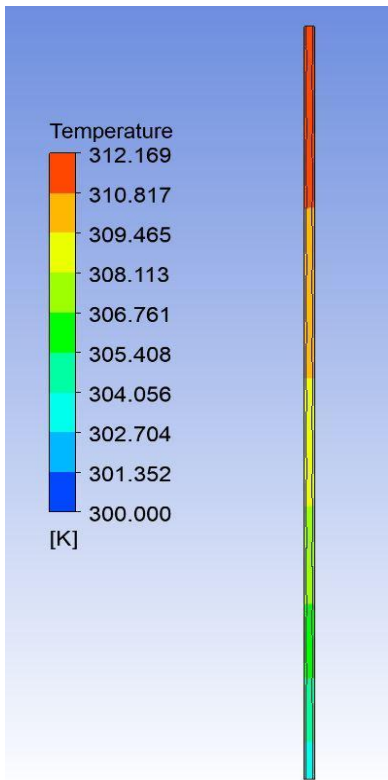

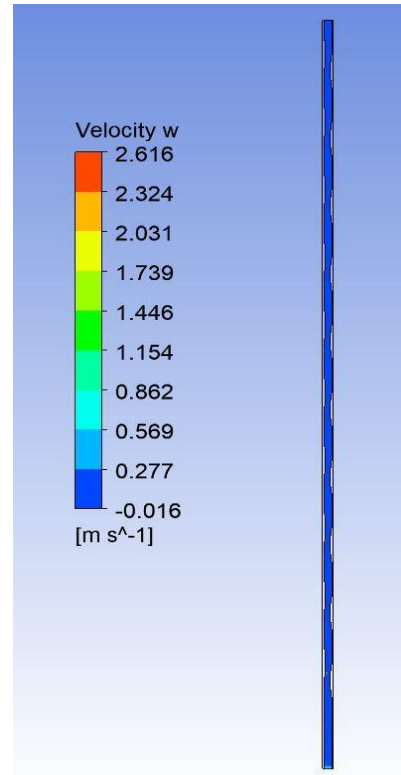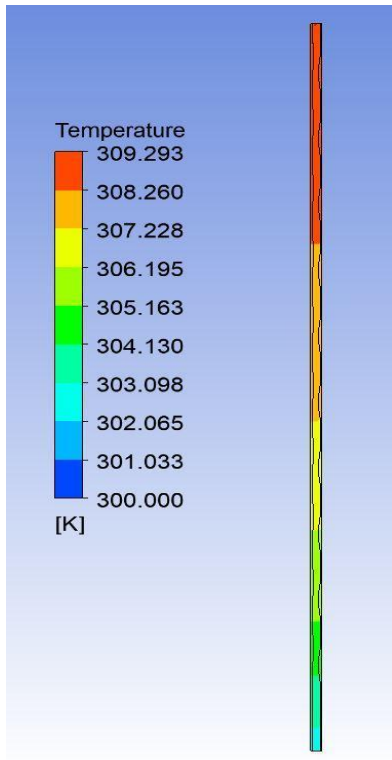*Fig 5.103 Temperature contour ARC6mm Re=1000*   *Fig 5.104 Velocity contour ARC6mm Re=1000*

Fig 5.105 Temperature contour ARC7mm Re=200   *Fig 5.106 Velocity contour ARC 7mmRe=200*
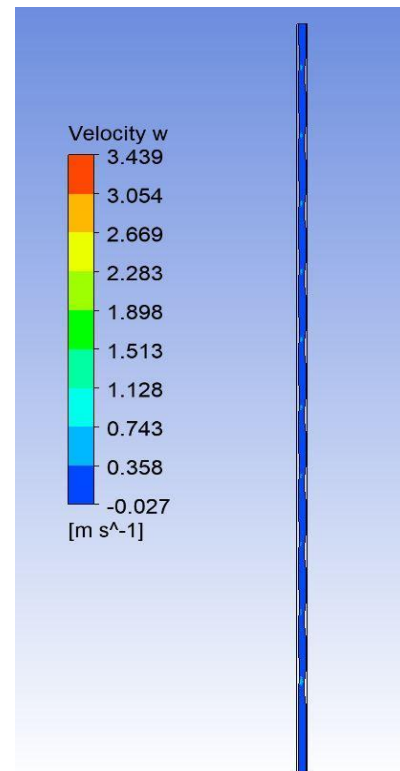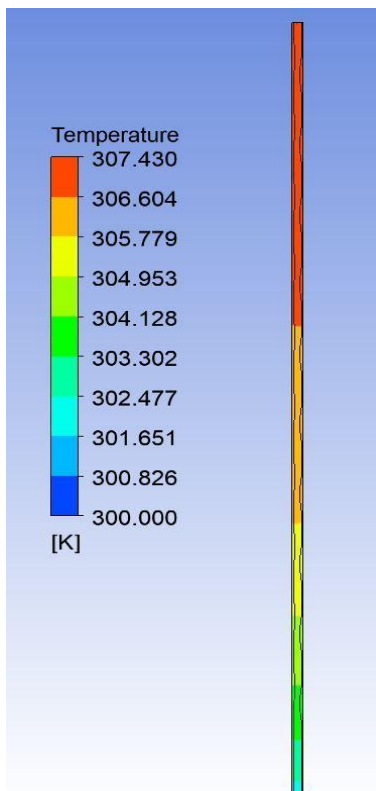

Fig 5.107 Temperature contour ARC7mm Re=400   *Fig 5.108 Velocity contour ARC7mm Re=400*

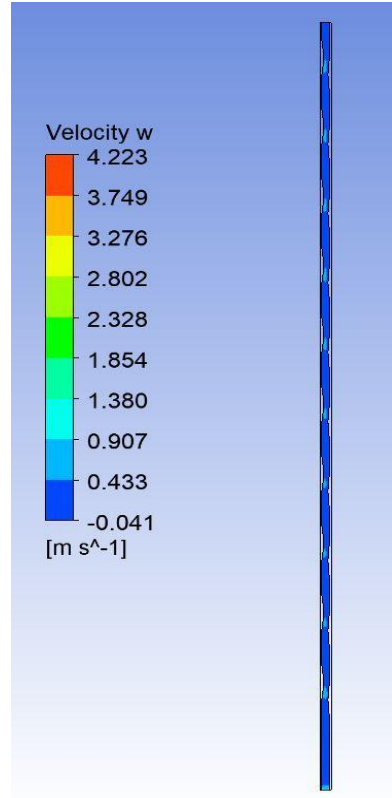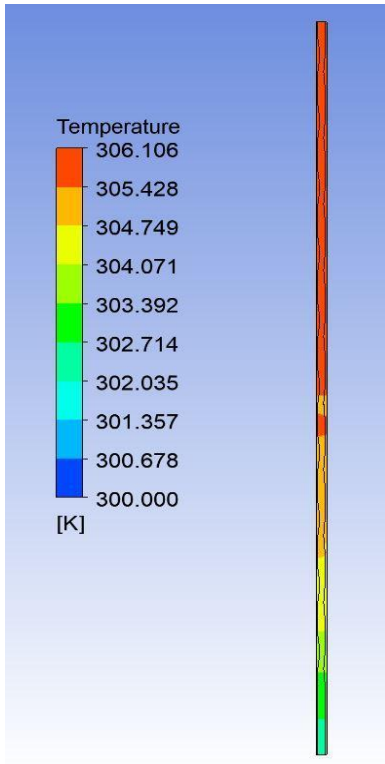*Fig 5.109 Temperature contour ARC 7mm Re=600*

Fig 5.110 Velocity contour ARC 7mmRe=600

Fig 5.111 Temperature contour ARC7mm Re=800

Fig 5.112 Velocity contour ARC7mm Re=800

Fig 5.113 Temperature contour ARC7mm Re=1000   Fig 5.114 Velocity contour ARC7mm Re=1000

Fig 5.115 Temperature contour ARC8mm Re=200   Fig 5.116 Velocity contour ARC8mm Re=200

Fig 5.117 Temperature contour ARC8mm Re=400   *Fig 5.118 Velocity contour ARC8mm Re=400*
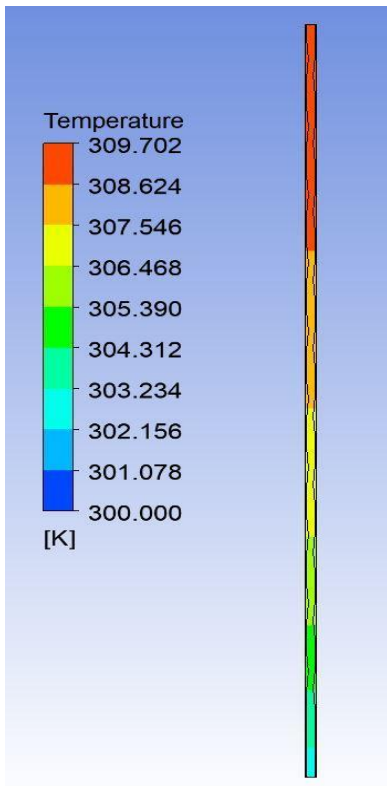
Fig 5.119 Temperature contour ARC8mm Re=600   *Fig 5.120 Velocity contour ARC8mm Re=600*
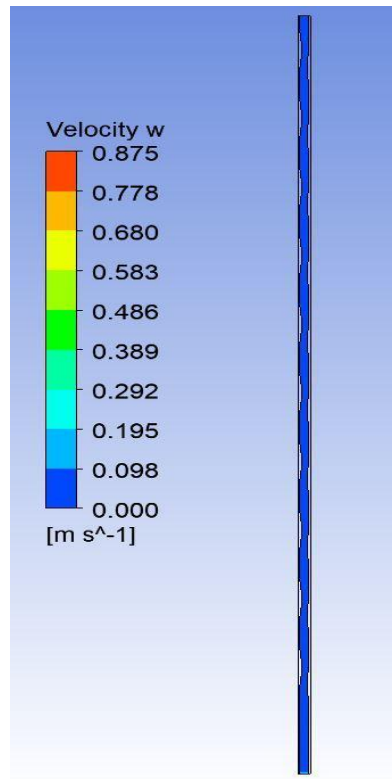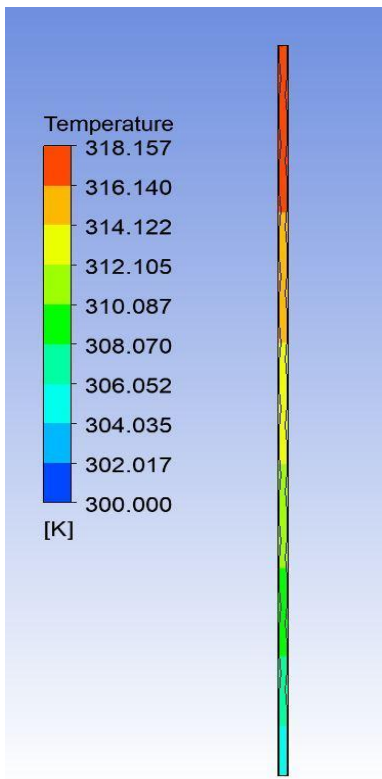
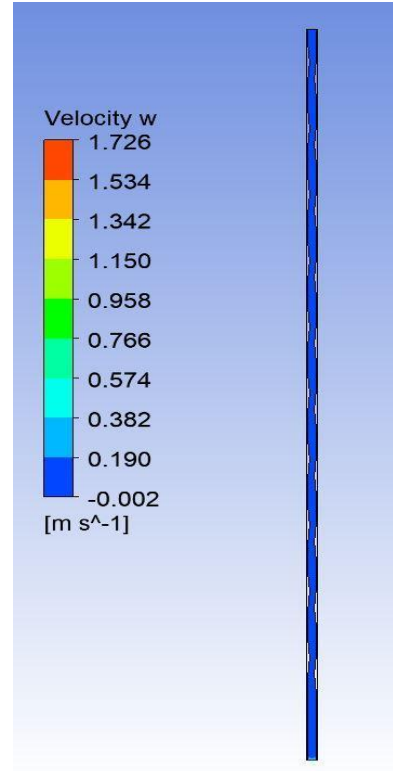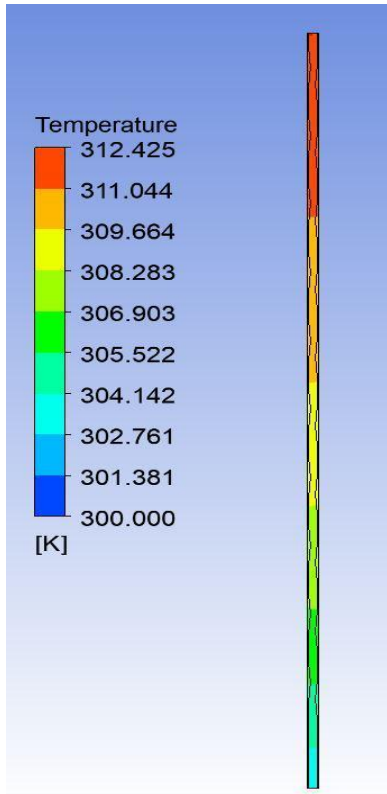*Fig 5.121 Temperature contour ARC8mm Re=800*   *Fig 5.122 Velocity contour ARC8mm Re=800*
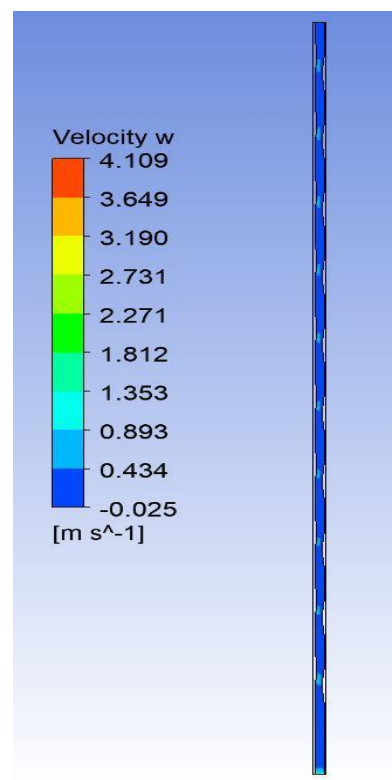
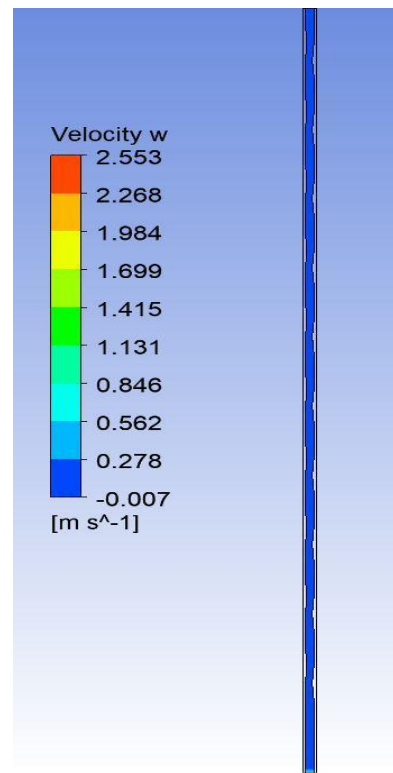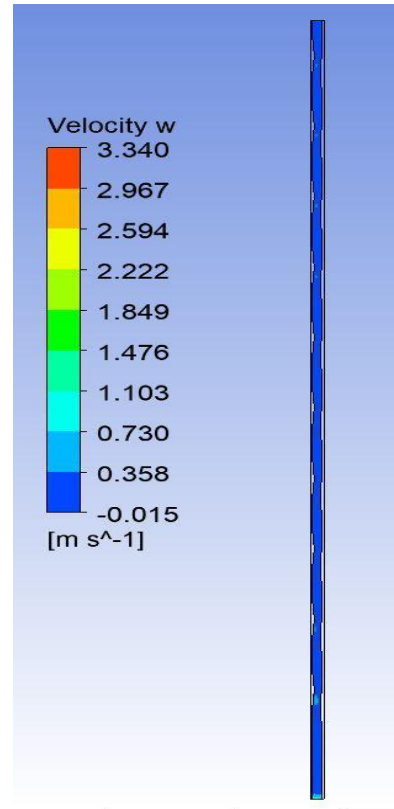*Fig 5.123 Temperature contour ARC8mm Re=1000*   *Fig 5.124 Velocity contour ARC8mm Re=1000*
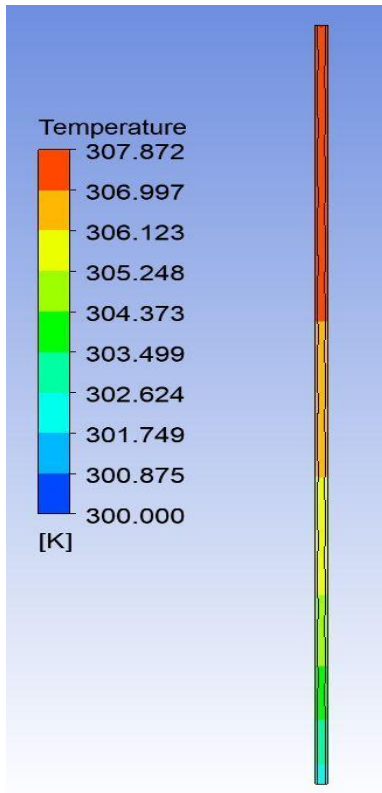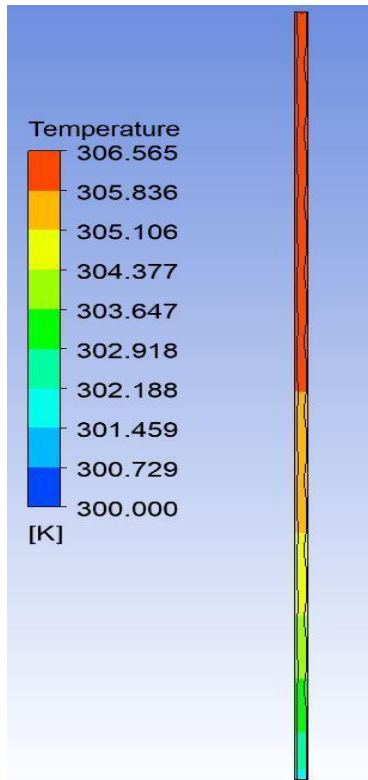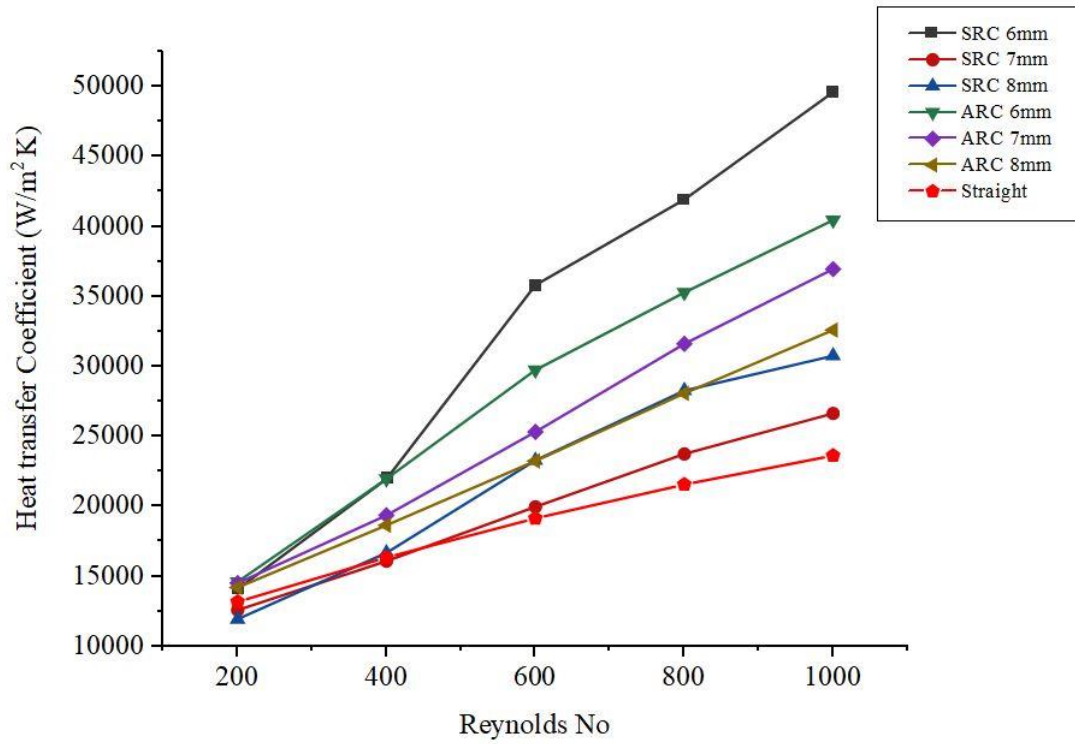
Fig 5.125 Graph for Ribbed Channel (Heat transfer Coefficient Vs Reynolds No)
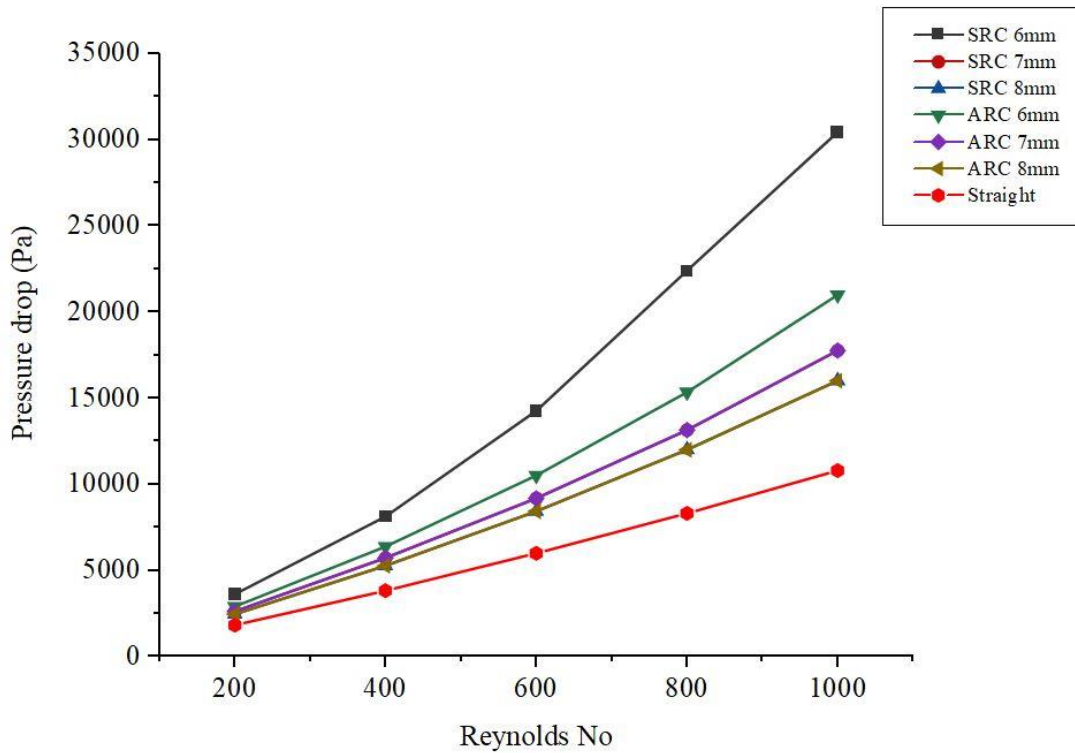
Fig 5.126 Graph for Ribbed Channel (Pressure drop Vs Reynolds No)
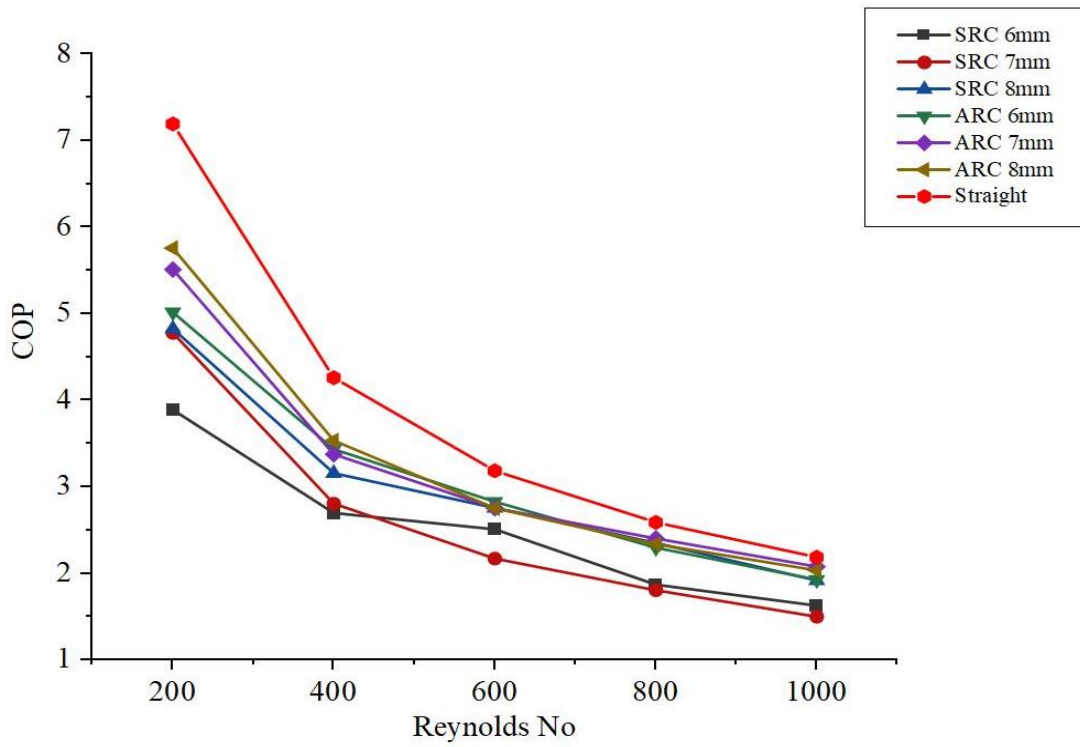
Fig 5.127 Graph for Ribbed Channel (Coefficient of performance Vs Reynolds No)
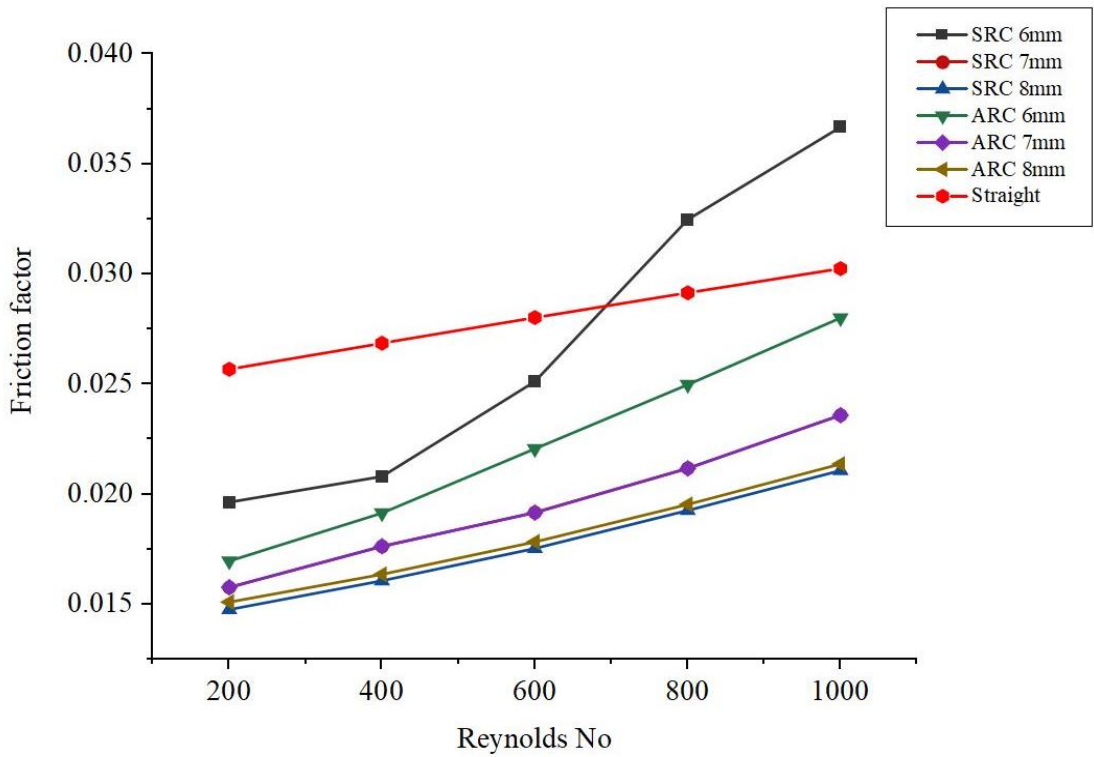
Fig 5.128 Graph for Ribbed Channel (Friction factor Vs Reynolds No)

- The heat transfer coefficient of the symmetric and asymmetric ribbed channels does not vary much with respect to the fillet radius of the microchannel
- The pressure drop of the symmetric microchannel is higher than the asymmetric microchannel
- The friction factor value ranges between 0.015 and 0.025 for symmetric and asymmetric ribbed microchannels
- On the whole, asymmetric ribbed channel having radius of rib=6 mm shows better results than symmetric ribbed microchannel in terms of Heat transfer coefficient. Since the pressure drop significance is not higher, so better flow characteristics are shown when Reynolds number ranges from 400 to 600

Asymmetric channel with R=6mm at Re=400	**Asymmetric channel with R=6mm at Re = 600**
h =21969.44 W/m^{2}K	h = 29752.35W/m^{2}K
ΔP = 6332.73 Pa	ΔP = 10518.8 Pa
friction factor = 0.0192	friction factor = 0.0221
COP = 3.4366	COP = 2.8285

CHAPTER-6

CONCLUSION

The present study investigates the performance of the microchannel heat sink for different flow path configurations. The following are the concluded results from the analysis

1. In general, Inclined fin microchannel is more effective in thermal performance when compared to the straight microchannel and Ribbed fin microchannel.

2. The main objective of this analysis is to have higher heat transfer characteristics and minimum pressure drop across the microchannel. With respect to the above statement, the Inclined fin channel and Asymmetric rib type are considered to be conservative.

3. Heat transfer coefficient of 90^0 inclined fin channel is 54% higher than Asymmetric rib channel of 8mm radius at Re=400 and 98% higher at Re=600

4. The pressure drop of 90° inclined fin channel is 20% higher than Asymmetric rib channel of 8mm radius at Re=400 and 38% higher at Re=600. But this pressure drop will not increase the pumping power significant.

5. Similar to the pressure drop, the friction factor variation is also not significant for all cases.

6. Based on the above inference, it is been said that 90° inclined fin channel can be used for the future study.

CHAPTER-7
REFERENCES

[1] Yogesh K. Prajapati 'Influence of fin height on heat transfer and fluid flow characteristics of rectangular microchannel heat sink'. International Journal of Heat and Mass Transfer Volume 137, July 2019, Pages 1041-1052.

[2] Dawei Zhuang, Yifei Yang, Guoliang Ding, Xinyuan Du, Zuntao Hu 'Optimization of Microchannel Heat Sink with Rhombus Fractal-like Units for Electronic Chip Cooling'. International Journal of Refrigeration, Volume 116, August 2020, Pages 108-118.

[3] K.Derakhshanpour, R.Kamali, M.Eslami 'Effect of rib shape and fillet radius on thermal-hydrodynamic performance of microchannel heat sinks'. International Communications in Heat and Mass Transfer, Volume 119, December 2020, Pages 108-118

[4] Fei Li, Qingming Ma, Gongming Xin, Jingchao Zhang, Xinyu Wang 'Heat transfer and flow characteristics of microchannels with solid and porous ribs. Applied Thermal Engineering, Volume 178, September 2020, 115639.

[5] Shi Zeng, Poh Seng Lee 'Topology optimization of liquid-cooled microchannel heat sinks: An experimental and numerical study'. International Journal of Heat and Mass Transfer Volume 142, October 2019, 118401.

[6] Qifeng Zhu, Huixue Xia, Junjie Chen, Xinmin Zhang a, Kunpeng Chang, Hongwei Zhang, Hua Wang, Jianfeng Wan, Yangyang Jin 'Fluid flow and heat transfer characteristics of microchannel heat sinks with different groove shapes. International Journal of Thermal Sciences, Volume 161, March 2021, 106721.

[7] Nicholas Gilmore, VictoriaTimchenko, Chris Menictas 'Open manifold microchannel heat sink for high heat flux electronic cooling with a reduced pressure drop' International Journal of Heat and Mass Transfer, Volume 163, December 2020, 120395.

[8] Lixiao Liang, Jibiao Hou, Xiangjun Fang, Ying Han, Jie Song, Le Wang, Zhanfeng Deng, Guizhi Xu, Hongwei Wu,(2019) ' Flow characteristics and heat transfer performance in Y-Fractal mini/microchannel heat sink', Case Studies in Thermal Engineering ,Vol.15,pp.1-9.

[9] Sanjeev Kumar, Pawan Kumar Singh, (2019), 'A novel approach to manage temperature non-uniformity in minichannel heat sink by using intentional flow maldistribution', Applied Thermal Engineering, Vol.163, pp.1-12.

[10] Vikas Yadav, Kuldeep Baghel, Ritunesh Kumar, S.T. Kadam 'Numerical investigation of heat transfer in extended surface microchannels'. International Journal of Heat and Mass Transfer, Volume 93, February 2016, Pages 612-622

[11] Ergin Bayrak, Ali Bahadir Olcay, Mustafa Fazil Serincan 'Numerical investigation of the effects of geometric structure of microchannel heat sink on flow characteristics and heat transfer performance'. International Journal of Thermal Sciences, Volume 135, January 2019, Pages 589-600.

[12] Hao Ma, Zhipeng Duan, Xiaoru Ning, Liangbin Su 'Numerical investigation on heat transfer behavior of thermally developing flow inside rectangular microchannels' Case Studies in Thermal Engineering Volume 24, April 2021, 100856.

[13] V.Murali Krishna Mechiri Sandeep, Kumar O.Mahesh, P.Senthil Kumar 'Numerical investigation of heat transfer and pressure drop for cooling of microchannel heat sink using MWCNT-CuO-Water hybrid nanofluid with different mixture ratio'. Materials Today: Proceedings, Volume 42, Part 2, 2021, Pages 969-974.

[14] Guilian Wang, Tao Chena, Ming fei, Tiana Guifu Ding 'Fluid and heat transfer characteristics of microchannel heat sink with truncated rib on sidewall'. International Journal of Heat and Mass Transfer Volume 148, February 2020, 119142.

[15] Ngoctan Tran, Yaw-Jen Chang, Jyh-tong, Tenga Ralph Greif 'A study on five different channel shapes using a novel scheme for meshing and a structure of a multi-nozzle microchannel heat sink' International Journal of Heat and Mass Transfer, Volume 105, February 2017, Pages 429-442.

[16] Ihsan Ali Ghani, Nor Azwadi Che Sidik, Natrah Kamaruzamana 'Hydrothermal performance of microchannel heat sink: The effect of channel design'. International Journal of Heat and Mass Transfer, Volume 107, April 2017, Pages 21-44.

[17] Liaofei Yin, Peixue Jiang, Ruina Xu, Haowei Hub Li Jia 'Heat transfer and pressure drop characteristics of water flow boiling in open microchannels'. International Journal of Heat and Mass Transfer, Volume 137, July 2019, Pages 204-215

[18] Liangbin Su, Zhipeng Duan, Boshu He, Hao Ma, Xiaoru Ning, Guangchao, Ding Yang Cao 'Heat transfer characteristics of thermally developing flow in rectangular microchannels with constant wall temperature' International Journal of Thermal Sciences, Volume 155, September 2020, 106412.